[5] P. Fontanari, M. Badier, C. Guillot, C. Tomei, H. Burnet, B. Gardette, Y. Jammes, Changes in maximal performance of inspiratory and skeletal muscles during and after the 7.1-MPa Hydra 10 record human dive, Eur. J. Appl. Physiol. 81 (2000) 325–328.
[6] S. Fukui, T. Ookawara, H. Nawashiro, K. Suzuki, K. Shima, Post-ischemic transcriptional and translational responses of EC-SOD in mouse brain and serum, Free Rad. Biol. Med. 32 (2002) 289–298.
[7] J. Hitomi, T. Katayama, M. Taniguchi, A. Honda, K. Imaizumi, M. Tohyama, Apoptosis induced by endoplasmic reticulum stress depends on activation of caspase-3 via caspase-12, Neurosci. Lett. 357 (2004) 127–130.
[8] T. Ikeda, Y.X. Xia, M. Kaneko, H. Sameshima, T. Ikenoue, Effect of the free radical scavenger, 3-methyl-1-phenyl-2-pyrazolin-5-one (MCI-186), on hypoxia–ischemia-induced brain injury in neonatal rats, Neurosci. Lett. 329 (2002) 33–36.
[9] S. Kuroda, B.K. Siesjö, Reperfusion damage following focal ischemia: pathophysiology and therapeutic windows, Clin. Neurosci. 4 (1997) 199–212.
[10] S. Love, Oxidative stress in brain ischemia, Brain Pathol. 9 (1999) 119–131.
[11] L.J. Martin, M.E. Blue, M.V. Johnston, Apoptosis has a prolonged role in the neurodegeneration after hypoxic ischemia in the newborn rat, J. Neurosci. 20 (2000) 7994–8004.
[12] T. Nakagawa, H. Zhu, N. Morishima, E. Li, J. Xu, B.A. Yankner, J. Yuan, Caspase-12 mediates endoplasmic-reticulum-specific apoptosis and cytotoxicity by amyloid β, Nature 403 (2000) 98–103.
[13] F.J. Northington, D.M. Ferriero, D.L. Flock, L.J. Martin, Delayed neurodegeneration in neonatal rat thalamus after hypoxia–ischemia is apoptosis, J. Neurosci. 21 (2001) 1931–1938.
[14] I. Ohsawa, M. Ishikawa, K. Takahashi, M. Watanabe, K. Nishimaki, K. Yamagata, K. Katsura, Y. Katayama, S. Asoh, S. Ohta, Hydrogen acts as a therapeutic antioxidant by selectively reducing cytotoxic oxygen radicals, Nat. Med. 13 (2007) 688–694.
[15] S.S. Sheu, D. Nauduri, M.W. Anders, Targeting antioxidants to mitochondria: a new therapeutic direction, Biochim. Biophys. Acta 1762 (2006) 256–265.
[16] K. Suzuki, S. Imajoh, Y. Emori, H. Kawasaki, Y. Minami, S. Ohno, Calcium-activated neutral protease and its endogenous inhibitor. Activation at the cell membrane and biological function, FEBS Lett. 220 (1987) 271–277.
[17] R.C. Vannucci, J.R. Connor, D.T. Mauger, C. Palmer, M.B. Smith, J. Towfighi, S.J. Vannucci, Rat model of perinatal hypoxic-ischemic brain damage, J. Neurosci. Res. 55 (1999) 158–163.
[18] H. Yao, G.G. Haddad, Calcium and pH homeostasis in neurons during hypoxia and ischemia, Cell Calcium 36 (2004) 247–255.

Neurobiology of Disease

Age-Dependent Neurodegeneration Accompanying Memory Loss in Transgenic Mice Defective in Mitochondrial Aldehyde Dehydrogenase 2 Activity

Ikuroh Ohsawa,[1,2] Kiyomi Nishimaki,[1] Yayoi Murakami,[1] Yuko Suzuki,[1] Masahiro Ishikawa,[1] and Shigeo Ohta[1]

[1]Department of Biochemistry and Cell Biology and [2]The Center of Molecular Hydrogen Medicine, Institute of Development and Aging Sciences, Graduate School of Medicine, Nippon Medical School, Kawasaki 211-8533, Japan

Oxidative stress may underlie age-dependent memory loss and cognitive decline. Toxic aldehydes, including 4-hydroxy-2-nonenal (HNE), an end product of lipid peroxides, are known to accumulate in the brain in neurodegenerative disease. We have previously shown that mitochondrial aldehyde dehydrogenase 2 (ALDH2) detoxifies HNE by oxidizing its aldehyde group. To investigate the role of such toxic aldehydes, we produced transgenic mice, which expressed a dominant-negative form of ALDH2 in the brain. The mice had decreased ability to detoxify HNE in their cortical neurons and accelerated accumulation of HNE in the brain. Consequently, their lifespan was shortened and age-dependent neurodegeneration and hyperphosphorylation of tau were observed. Object recognition and Morris water maze tests revealed that the onset of cognitive impairment correlated with the degeneration, which was further accelerated by APOE (apolipoprotein E) knock-out; therefore, the accumulation of toxic aldehydes is by itself critical in the progression of neurodegenerative disease, which could be suppressed by ALDH2.

Key words: ALDH2; HNE; memory loss; mitochondria; oxidative stress; transgenic mice

Introduction

A decline in cognitive function is associated with aging, mainly as a result of oxidative stress in the brain (Mattson, 2004). Reactive oxygen species (ROS), strong oxidizing molecules including hydroxyl radicals, modify proteins, nucleic acids, and polyunsaturated fatty acids of the lipid membrane, and injure cells. Lipid peroxidation leads to the formation of highly reactive α,β-unsaturated aldehydes, primarily malondialdehyde and 4-hydroxy-2-nonenal (HNE) (Schneider et al., 2001). In particular, HNE is a strong electrophile and has the ability to readily adduct and damage proteins (Uchida, 2003). The accumulation of HNE-adducted proteins in pyramidal neurons has been observed in the brains of patients with Alzheimer's disease (AD) and Parkinson's disease (Yoritaka et al., 1996; Lovell et al., 1997; Montine et al., 1997; Sayre et al., 1997). HNE application *in vitro* mimics the pathological changes noted in AD, including modification of tau (Takeda et al., 2000; Liu et al., 2005) and β-amyloid (Murray et al., 2007), inhibition of the glucose transporter (Reagan et al., 2000), and microtubular disruption (Gadoni et al., 1993), and eventually leads to cell death (Mark et al., 1997).

HNE is adducted with glutathione via glutathione *S*-transferase (Xie et al., 1998), oxidized by aldehyde dehydrogenase (ALDH) to form 4-hydroxy-2-noneoate (Tjalkens et al., 1999), or reduced by aldo-keto reductase, alcohol dehydrogenase (ADH) or amyloid β-peptide-binding ADH (ABAD) to form 1,4-dihydroxynonene (Srivastava et al., 1998; Murakami et al., 2008). These multiple pathways are used to detoxify HNE in cells (Siems and Grune, 2003). We found previously that mitochondrial ALDH2-deficient neuronal cells exhibited increased vulnerability to HNE (Ohsawa et al., 2003a). The cells accumulated HNE and showed decreased resistance to oxidative insult, suggesting that ALDH2 functions as a protector against oxidative stress by oxidizing HNE. However, ALDH2 is well known to oxidize acetaldehyde produced from ethanol into acetate (Higuchi et al., 2004). A mutant allele, *ALDH2*2*, has a single point mutation (G→A) in exon 12 of the active *ALDH2*1* gene and is confined to Asians. This mutation results in a substitution of glutamate 487 to lysine (E487K), acting in a dominant-negative manner (Bosron and Li, 1986). Individuals with the *ALDH2*2* allele exhibit the alcohol-flushing syndrome attributable to an elevated blood acetaldehyde level.

We reported previously that a molecular epidemiological analysis revealed a higher concentration of lipid peroxides (LPOs) in the sera of ALDH2-deficient females than in those carrying an active ALDH2 (Ohsawa et al., 2003b), and that ALDH2 deficiency is a risk factor for late-onset AD, synergistically acting with the $\varepsilon 4$ allele of the apolipoprotein E gene (*APOE-ε4*) (Kamino et al., 2000). This finding was recently confirmed by studies in China and Korea (Jo et al., 2007; Wang et al., 2008). To verify the role of ALDH2-deficiency in age-associated

Received Nov. 5, 2007; revised May 2, 2008; accepted May 4, 2008.

This work was supported by grants from the Ministry of Health, Labour and Welfare (Longevity Science, H17-Chouju-009; Nervous and Mental Disorders, 17A-10) (S.O.).

Correspondence should be addressed to Shigeo Ohta, Department of Biochemistry and Cell Biology, Institute of Development and Aging Sciences, Graduate School of Medicine, Nippon Medical School, 1-396 Kosugi-cho, Nakahara-ku, Kawasaki 211-8533, Japan. E-mail: ohta@nms.ac.jp.

DOI:10.1523/JNEUROSCI.4956-07.2008

 0270-6474/08/286239-11$15.00/0

neurodegenerative diseases, we examined physiological changes, and learning and memory impairments by using transgenic (Tg) mice expressing ALDH2*2 in the brain. Here, we show that ALDH2-deficient mice present with age-dependent signs of neurodegeneration such as loss of pyramidal cells, activation of glial cells, and prominent deficits in cognition.

Materials and Methods

Transgenic mice. To generate Tg mice that express ALDH2*2, a transgene containing a mouse version of *ALDH2*2* under the control of the human elongation factor-1α (EF1α) promoter was constructed. A DNA fragment containing *ALDH2*2* in plasmid pBluescript SK (Ohsawa et al., 2003a) was digested with *Xba*I and inserted into the *Xba*I site of plasmid pEF1-BOS (Mizushima and Nagata, 1990). The 4.2 kb *Apa*LI–*Pvu*I fragment of EF1α promoter-*ALDH2*2* derived from the resultant plasmid was purified and dissolved in TE buffer at a concentration of 3 μg/ml. Tg mice were produced in accordance with a standard procedure. In brief, the DNA fragment was microinjected into 800 fertilized eggs taken from superovulated C57BL/6 females. The injected eggs were surgically transferred to the oviducts of C57BL/6 pseudopregnant females to produce male chimeric mice. Sixteen mice carrying the transgene were selected by PCR of tail DNA with primers 5′-NNTCTAGAGCCACCATGGCT-CAGGGCGCCCATA and 5′-GAAGGGTTGACGGTGGGAAATGTT. F_1 heterozygous animals were backcrossed to C57BL/6 mice for more than five generations, and homozygous mice (*ALDH2*2*$^{+/+}$) were finally obtained. Next, three independent lines (DAL101, DAL102, and DAL103) were selected according to the expression of *ALDH2*2* in the brain determined by the following method. Poly(A)$^+$ RNA was extracted from the brain and mismatch reverse transcription (RT)-PCR was performed with *ALDH2*-specific primers 5′-AGATGTCAGGGAGTGG-CAGG (see Fig. 1, primer A) and 5′-GTGGCACTTTGACAGTAA-CCGTCTTAACGT (see Fig. 1, primer B). The amplified cDNA fragment was incubated with *Acl*I and subjected to PAGE. Two digested fragments (54 and 30 bp) were derived from exogenous *ALDH2*2*, whereas the fragment not digested with *Acl*I (84 bp) was from endogenous *ALDH2*. To quantify the expression of *ALDH2* and *ALDH2*2* transcripts in each region of the brain, their cDNA was qualified by ABI7700 with real-time RT-PCR primers and probe 5′-ACCTGTCCCAAGCTCTGCAG, 5′-GGAGACTGGGCCCCAAAC, and 5′-CTGGCACTGTGTGGATC-AACTGCTACG for endogenous *ALDH2*, and 5′-AAAACC-CAACAAGATATACTGAGAAAAAC, 5′-GACCTGATACTCTCA-AGGGTCCC, and 5′-CACTGTCTAGAGTGAGGGTCCCCACCTG for exogenous *ALDH2*2*. DAL101 was further mated with *ApoE*$^{-/-}$ mice (purchased from Taconic Farms) and offspring carrying the genotype *ALDH2*2*$^{+/+}$/*ApoE*$^{-/-}$ were obtained.

All mice were kept on a 12 h light/dark cycle with *ad libitum* access to food and water. The studies were approved by the Animal Care and Use Committee of Nippon Medical School. All experiments were performed by examiners blinded to the genotypes or treatments of the mice.

Primary culture of neurons. Primary cultures of cortical neurons were prepared from 17 d mouse embryos by the method described previously (Ohsawa et al., 2007). In brief, neocortical tissue was cleaned of meninges, minced, and treated with trypsin. After mechanical dissociation by pipetting, cells were resuspended in DMEM (Invitrogen) supplemented with insulin (5 μg/ml), transferrin (5 μg/ml), putrescine (100 μM), selenium (5 ng/ml), and penicillin–streptomycin, and then plated onto poly-L-lysine-coated plates at a density of 5×10^4 cells/cm^2. After 3 d of the culture, we used neurons for analysis of cell viability. For preparing hippocampal cells, hippocampus of 17 d mouse embryo was cleaned of meninges, minced, and treated with protease mixture (SUMILON). After mechanical dissociation by pipetting, we resuspended cells in nerve cell culture medium (SUMILON), and then plated onto poly-L-lysine-coated plates at a density of 5×10^4 cells/cm^2, changed one-half of the medium once every 2 d, and then used neurons at day 1 and day 9 for analysis of neurite outgrowth and cell viability, respectively. Neuronal identity was confirmed by immunostaining with the neuron marker anti-TUJ-1 (Covance) and/or anti-MAP2 (Sigma-Aldrich) and astrocyte marker anti-glial fibrillary acidic protein (GFAP) (ThermoImmunon) antibodies. After incubation with BODIPY FL goat anti-mouse IgG (Invitrogen), cells were imaged by confocal scanning microscopy (Olympus) using excitation and emission filters of 488 and 510 nm, respectively. Preparations containing >90% neurons were used for experiments. Apoptosis was detected by DNA strand breaks using terminal deoxynucleotidyl transferase-mediated biotinylated UTP nick end-labeling (TUNEL) according to the procedure of the manufacturers (MBL).

Preliminary observation and neurological reflexes. Mice were first observed in their home cages for general activity and levels of aggression. Each mouse was then observed in a bare cage for general health, presence of whiskers, and appearance of fur. Mice were challenged to evaluate reflex responses including eye blink, ear twitch, whisker touch, and righting reflexes (Miyakawa et al., 2001).

Open-field test. Locomotor activity was measured using an open-field apparatus (45 × 45 × 65 cm) (Kim et al., 2006). Animals were placed in the center of the apparatus in standard indoor-lighting conditions and total distance traveled for 10 min was recorded. Between sessions, the apparatus was wiped clean with 70% ethanol.

Wire hanging test. The neuromuscular strength was tested by the wire hanging test (Hamann et al., 2003). In brief, mice were placed on a wire netting, which was lightly shaken, causing the mouse to grip the wire. After a 5 s cutoff time, the wire netting was turned upside down (180°) and the latency to fall was recorded for the maximum time.

Immunohistochemistry. The brain was removed and left one was kept at −80°C for biochemical assay. The right brain was further fixed for 4 h at room temperature by using 4% paraformaldehyde in PBS and subsequently cryoprotected with 30% sucrose in PBS. Frozen brain was sectioned at 8 μm thickness using a cryostat (Leica), mounted on slides, and air-dried. To stain sections with antibodies against NeuN (clone A60; Millipore), GFAP, and phospho-Tau (clone AT8; Pierce), the M.O.M. kit (Vector Laboratories) was used by the method according to the manufacturer. For double staining with anti-NeuN, antimonoclonal antibody and rabbit anti-GFAP polyclonal antibody (Abcam), we used Texas Red goat anti-mouse IgG (Invitrogen) and BODIPY FL goat anti-rabbit IgG (Invitrogen) as secondary antibodies and visualized signals with a laser-scanning confocal microscope.

Immunoblot analysis. The left hippocampus was dissected and Dounce-homogenized in cold lysate buffer [10 mM Tris, pH 7.4, 320 mM sucrose, 1% Triton X-100, 1% CHAPS (3-[(3-cholamidopropyl)-dimethylammonio]-1-propanesulfonate), 0.025% NaN_3, 1 mM EDTA, 1 mM EGTA, 50 mM sodium fluoride, 2 mM sodium orthovanadate, and protease inhibitor Complete tablets EDTA-free (Roche)] and stored at −80°C. Protein concentration was determined with the BCA protein assay kit (Pierce). Equal amounts of protein (100 μg) were separated on 10–20% polyacrylamide gels (Daiichi), transferred onto PolyScreen transfer membranes (PerkinElmer), and incubated in blocking buffer consisting of TBS (10 mM Tris, pH 7.6, and 150 mM NaCl) with 5% bovine serum albumin. For immunodetection of specific bands on the blots, Can Get Signal immunoreaction enhancer solution (Toyobo) was used by the method according to the manufacturer. Blots were incubated with primary antibodies to tau phospho-Ser-202/205 (AT-8; 1:500; Pierce), pan-tau (TAU-5; 1:1000; Millipore), p35 and p25 C terminus (C-19; 1:200; Santa Cruz), and cyclin-dependent kinase 5 (Cdk5) (C-8; 1:100; Santa Cruz) and further incubated with alkaline phosphatase-conjugated secondary antibodies (1:10,000; Cappel). Signals were visualized with AttoPhos substrate (Roche). Blots were stripped with stripping buffer (62.5 mM Tris, pH 6.8, 100 mM 2-mercaptoethanol, 2% SDS) and reprobed with antibody to β-actin (1:10,000; Sigma-Aldrich) to normalizing the amounts of loaded proteins.

HNE concentration. Concentration of HNE in the brain was determined using a colorimetric assay kit (HAE-586; OXIS International) according to the manufacturer's instructions. The protein concentration of each sample was measured using a BCA protein assay reagent (Pierce).

Visual object recognition test. The visual object recognition test (vORT) was used to test recognition memory (Wang et al., 2004). Mice were first habituated in a 25 × 40 cm cage for 6 h before training. During 10 min of training, two plastic blocks with different shapes and colors were presented. Object recognition was scored by the number of approaches to

and/or sniffs of the object and was reported as percentage preference (recognition index). One day after training, one of the conditioned blocks was replaced with a novel object to test for memory retention, and recognition index was scored during 5 min of testing.

Water maze test. The apparatus used for water maze tasks was a circular pool (1.5 m diameter) painted white and filled with water maintained at 25°C, and rendered opaque by the addition of nontoxic white paint. The maze is located in a room containing several simple visual, extramaze cues. Mice were trained in the morning to swim to a 10-cm-diameter circular clear acryl resin platform submerged 1 cm beneath the surface of the water and invisible to the mice while swimming. Mice were monitored by a camera mounted above the pool, and all trials were stored on PC for subsequent analysis. In each trial, the mouse was placed and released into the pool at one of four designated start points in a pseudorandom order and allowed to find and escape to the submerged platform and remain there for 20 s. If a mouse failed to find the platform within 60 s, it was guided carefully to the platform and allowed to remain there for 20 s. After this, each mouse was dried gently with a towel and placed into a holding cage for 30 min until the start of next trial. Mice were given four trials a day for 5 d. Retention of the spatial training was assessed 1 h after the last training trial. A single probe trial consisted of a 60 s free swim in the pool without the platform. Mice were placed and released at the location opposite the site where the platform had been located and the time spent in each quadrant was recorded. Finally, after the probe trial, a visible platform was placed in the training quadrant 1 cm above the surface of the water. As in the place-learning task, the escape latencies were measured during at least four trials per session except that the test was conducted in a single day.

Statistical analysis. We performed statistical analyses using StatView software (SAS Institute) by applying an unpaired two-tailed Student's *t* test and ANOVA followed by Fisher's exact test for single and multiple comparisons, respectively. To calculate survival curves, the Kaplan–Meier method was used and the survival periods were compared with the log rank test (Mantel–Cox) for univariate analysis. We performed experiments for quantification in a blinded manner.

Results

Expression of ALDH2*2 in the brain and vulnerability of ALDH2*2-expressing neurons to HNE

The mouse version of the dominant-negative form of ALDH2 (ALDH2*2) was introduced under an EF1α promoter (Fig. 1*A*), which constitutively expresses genes in most tissues (Wakabayashi-Ito and Nagata, 1994). Because the expression extent depends on the location inserted, we paid attention to the expression of ALDH2*2 in the brain and selected three independent transgenic founders (DAL101, DAL102, and DAL103) and confirmed expression of ALDH2*2 by RT-PCR in the brain (Fig. 1*B*). One founder (DAL101), which expressed the highest amount of ALDH2*2, was maintained as homozygotes and mainly used for additional experiments. The amount of exogenous ALDH2*2 transcripts relative to endogenous ALDH2 transcripts was higher in the olfactory bulb, cortex, hippocampus, and midbrain in DAL101 (Fig. 1*C*).

To evaluate the effect of ALDH2*2 in neurons, we examined the ability of HNE detoxification and found that exposure to HNE resulted in a more rapid decrease of viable cells in the ALDH2*2-expressing neurons. At first, hippocampal neurons were prepared from embryonic 17 d DAL101. Moderate neuritogenesis was seen after 1 d in culture. Then, cells were treated with HNE and incubated for an additional 1 d. Immunostaining with anti-MAP2 antibody showed that neurite length of neurons prepared from DAL101 was shorter than that from non-Tg control (CTL) mice (C57BL/6) (Fig. 2*A*,*B*). After 9 d in culture, when a mature synaptic network was established, the hippocampal neurons were treated with HNE and further incubated for 1 d. Immunostaining with anti-MAP2 antibody revealed that the MAP2-positive neurites derived from DAL101 mice were decreased by the treatment with 3 μM HNE (Fig. 2*C*,*D*). Additionally, apoptosis was more induced by the treatment with HNE in neurons derived from DAL101 mice (Fig. 2*E*,*F*). Furthermore, cortical neurons were prepared from embryonic 17 d DAL101 and cultured for 3 d. Twenty-four hours after treatment with 1 μM HNE, 77.1% of ALDH2*2-expressing neurons were injured and detached from the dish, whereas control neurons prepared from CTL mice were attached and showed normal morphology with neuron-specific TUJ-1-positive neurites (Fig. 2*G*). The sensitivity of ALDH2*2-expressing neurons to HNE was dose-dependent (Fig. 2*H*). At that time, a higher amount of HNE was accumulated in ALDH2*2-expressing neurons (Fig. 2*I*), indicating that the metabolism ability of exogenous HNE decreased. These findings clearly show that the decline of ALDH2 activity makes neurons less resistant to HNE.

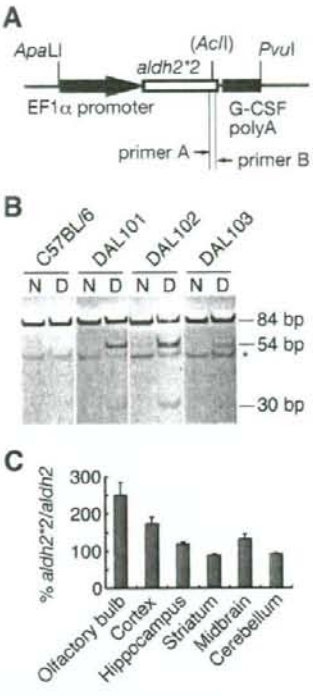

Figure 1. Generation of DAL mice. ***A***, Schematic drawing of the transfected DNA fragment. DAL mice were generated by the injection of 4.2 kb *ApaLI–PvuI* fragment into fertilized eggs. ***B***, RT-PCR analysis revealed that three transgenic founders expressed exogenous *ALDH2*2* in the brain. For PCR, primers shown in ***A*** were used (see Materials and Methods). The obtained PCR fragments (N) were digested with *AclI* (D). Two short fragments (54 and 30 bp) were derived from exogenous *ALDH2*2*, whereas the nondigested fragment was from endogenous *ALDH2*. *Nonspecific bands. ***C***, In the brain of DAL101, real-time RT-PCR analysis revealed more exogenous *ALDH2*2* transcripts relative to endogenous *ALDH2* transcripts in the olfactory bulb, cortex, hippocampus, and midbrain. Data are mean ± SEM ($n = 4$).

Accumulation of HNE in the brain is accelerated and lifespan is shortened

To clarify the relationship of ALDH2*2-expressing neurons with HNE, we measured HNE in the brain and found that a higher amount of HNE was accumulated in the brain of old DAL mice

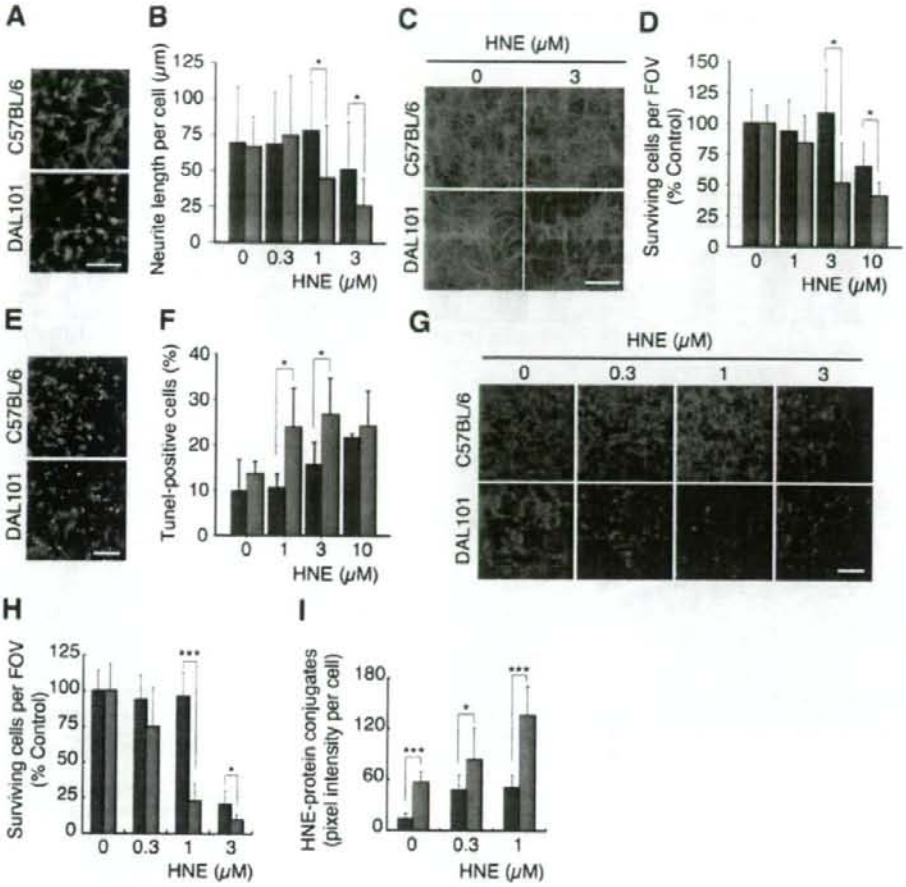

Figure 2. Neuronal vulnerability of DAL mice against HNE and its accumulation in the brain. Primary-cultured cells isolated from the brain of DAL101 (red bar) and C57BL/6 (blue bar) were treated with HNE and further incubated for 1 d. ***A***, ***B***, After 1 d in culture, hippocampal cells were treated with 1 μM (***A***) or the indicated amount (***B***) of HNE and immunostained with the dendrite-specific antibody to MAP2. Scale bar, 100 μm. Neurite length of each cell was measured under a microscope in at least 10 cells per well (mean ± SD; $n = 4$). *$p < 0.05$. ***C***, ***D***, Nine days after the culture, hippocampal cells were treated with the indicated amount of HNE and immunostained with anti-MAP2 antibody. Scale bar, 100 μm. Dead cells were washed out in the staining procedure and living cells were enumerated under a fluorescent microscope in four fields of view (FOVs) per well (mean ± SD; $n = 4$). *$p < 0.05$. ***E***, ***F***, Nine days after the culture, hippocampal cells were treated with 1 μM (***E***) or the indicated amount (***F***) of HNE and stained with TUNEL (green) and propidium iodide (PI) (red). Scale bar, 100 μm. Quantification of TUNEL-positive cells was performed under a fluorescent microscope in four FOVs per well and compared with the total number of cells (analyzed by PI staining) (mean ± SD; $n = 4$). *$p < 0.05$. ***G***, ***H***, Three days after the culture, cortical cells were treated with the indicated amount of HNE and surviving neurons were fixed and immunostained with the neuron-specific antibody to TUJ-1. Scale bar, 200 μm. Dead cells were washed out in the staining procedure, and living cells were enumerated under a fluorescent microscope in four FOVs per well (mean ± SD; $n = 4$). *$p < 0.05$; ***$p < 0.001$. ***I***, HNE–protein conjugates were calculated from pixel intensity in cells stained with anti-HNE antibody. Intensity was measured with NIH Image (mean ± SD; $n = 4$). *$p < 0.05$; ***$p < 0.001$.

(Fig. 3*A*). These results indicated that ALDH2*2 inhibited the degradation of HNE and enhanced oxidative stress in the brain.

One year after birth, female DAL101 showed no differences in weight (Fig. 3*B*), general health, sensory responses, or locomotor activity (Fig. 3*C*); however, male DAL mice showed muscle weakness (Fig. 3*D*) and some hair decolorization ($n = 8$ of 8) (Fig. 3*E*,*F*). It is noteworthy that the median lifespan of DAL101 was significantly shorter than that of CTL mice (96 vs 126 weeks; $p < 0.0001$) (Fig. 3*G*). The maximal lifespan of DAL101 was 129 weeks compared with 153 weeks for the CTL mice. The causes of death were not determined in many cases. In all the cases, no inflammation, other indicators of infectious disease, or tumors above levels seen in DAL mice were found.

ALDH2 deficiency by itself induces age-dependent brain degeneration

To examine whether ALDH2 deficiency induces neurodegeneration, we looked for abnormal neuronal loss in aged DAL mice by hematoxylin and eosin (H&E) staining and found the degeneration (Fig. 4*A–D*) and decrease in pyramidal neurons in the CA1 region of the hippocampus (Table 1). At 1 year of age, 20% of DAL mice showed neurodegeneration, whereas CTL mice did not (1 of 5 DAL vs 0 of 5 CTL; $p = 0.2918$). At 1.5 year of age, 77.8% of DAL mice showed neurodegeneration, whereas CTL mice did not (7 of 9 DAL vs 0 of 8 CTL; $p = 0.0053$). The obvious neurodegeneration in a 1 year DAL mouse was similar to that in 1.5 year DAL mice. In the hilus of the dentate gyrus of aged DAL mice, the

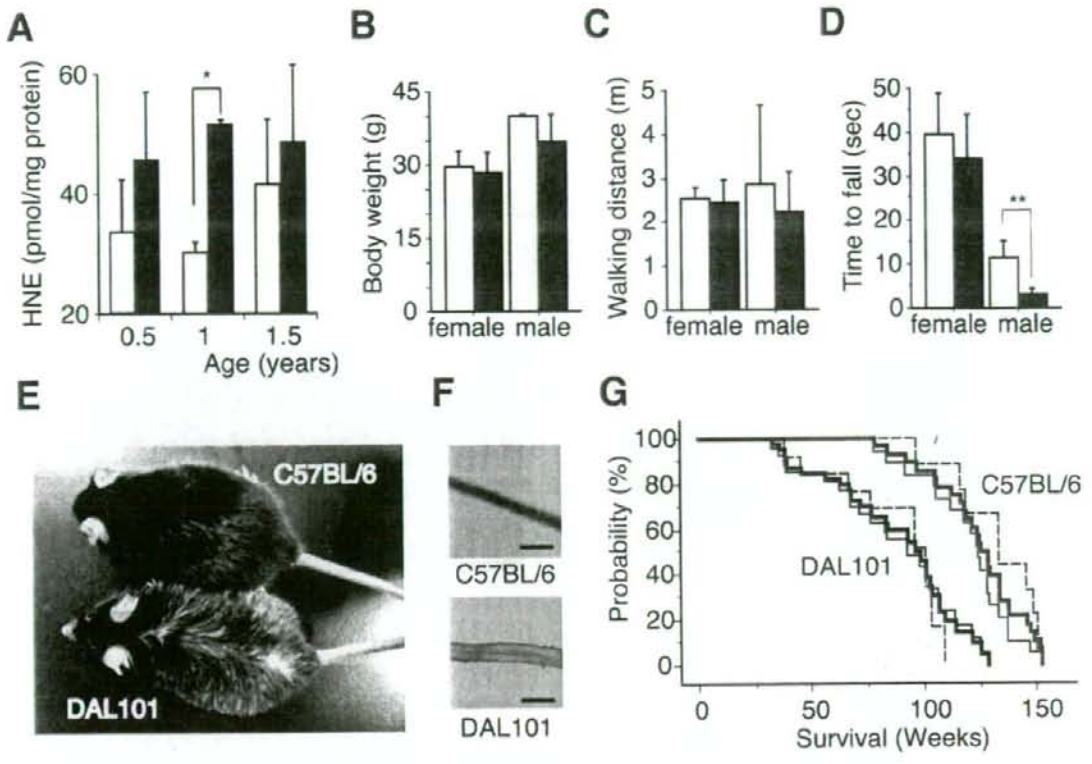

Figure 3. Characterization of DAL mice. ***A***, A higher amount of HNE was accumulated in the brain of DAL101 in an age-dependent manner. Filled bars, DAL101; open bars, C57BL/6. HNE levels were normalized against protein contents (mean ± SD; $n = 6$). *$p < 0.05$. ***B***, No significant difference in body weight was found between 1-year-old DAL101 (filled bars) and C57BL/6 (open bars) (mean ± SD; $n = 4$). ***C***, No significant difference in walking distance in the open-field test was found between 1-year-old DAL101 (filled bars) and C57BL/6 (open bars) (mean ± SD; $n = 4$). ***D***, Time to exhaustion and fall in hang test. Significant muscle weakness between 1-year-old DAL101 (filled bars) and C57BL/6 (open bars) was found in male (mean ± SD; $n = 4$). **$p < 0.01$. ***E***, ***F***, Hair decolorization in 1-year-old male DAL101. Scale bar, 50 μm. ***G***, Kaplan–Meier curve representing the survival of DAL101 and C57BL/6. Significant shortening of lifespan was found in DAL101 mice ($p < 0.0001$). Bold lines, Total male and female mice; thin line, male mice; thin dotted line, female mice.

neurons were also decreased (Table 1). Neuronal loss in the CA1 area of DAL mice was confirmed by immunostaining with anti-NeuN antibody (Tang et al., 2005) (Fig. 4*E–H*). Furthermore, marked increase in immunostaining with anti-GFAP antibody, a marker of activation of astrocytes, was found in the hippocampus of old DAL mice. At 1 year of age, 60% of DAL mice showed activation of astrocytes, whereas CTL mice did not (3 of 5 DAL vs 0 of 5 CTL; $p = 0.1667$). At 1.5 year of age, 55.6% of DAL mice showed activation of astrocytes, whereas CTL mice did not (5 of 9 DAL vs 0 of 8 CTL; $p = 0.0447$) (Fig. 4*I*,*J*). Because the increase of reactive astrocytes is a sensitive marker of brain injury (Isacson et al., 1987), these results indicate obvious impairment in neuronal function in these mice. As expected, we found neither the neuronal degeneration nor increase in reactive astrocytes in the brain of DAL mice at 6 months of age (Fig. 5, Table 1).

Next, we focused on the hyperphosphorylation of the tau protein. Tau-related pathologies are hallmarks of AD and other tauopathies (Takashima, 2006), and have been characterized in mice (Liou et al., 2003). The antibody, AT8, requires serine 202 to be phosphorylated to generate its epitope and is used frequently to assess the hyperphosphorylation of tau (Biernat et al., 1992). Staining brain sections of DAL mice at 1 and 1.5 year of age with AT8 yielded labeling of pyramidal neurons in the hippocampus of 44.4% of DAL mice, whereas those of wild-type littermates did not (4 of 9 DAL vs 0 of 13 CTL; $p = 0.0361$) (Fig. 4*K*,*L*). No obvious alternation was observed in the other brain regions. Immunoblot analysis also confirmed an increase in hyperphosphorylation of tau at the AT-8 site in the hippocampus of DAL mice (Fig. 4*M*). We examined the relationship between the DAL mice-specific increase in hyperphosphorylation of tau and expression levels of Cdk5 activator p25, p35, and Cdk5 (Cruz and Tsai, 2004); however, no obvious change in p25, p35, and Cdk5 levels was observed (Fig. 4*M*), suggesting that the other putative factors contribute to the abnormal hyperphosphorylation of tau in DAL mice.

Onset of cognitive impairment correlates with brain degeneration

To examine whether ALDH2 deficiency affects cognitive impairments, three independent genetic lines (DAL101, DAL102, and DAL103) were applied to the simple vORT. Because of relatively low physical demands in the test, male mice were used (Fig. 3*D*). Memory formation depends on the hippocampus (Miyamoto et al., 2005). During 10 min of training, two objects (global, a; triangle, b) were presented to a mouse. C57BL/6 mice, which were used as a control, and all DAL mice approached or sniffed each

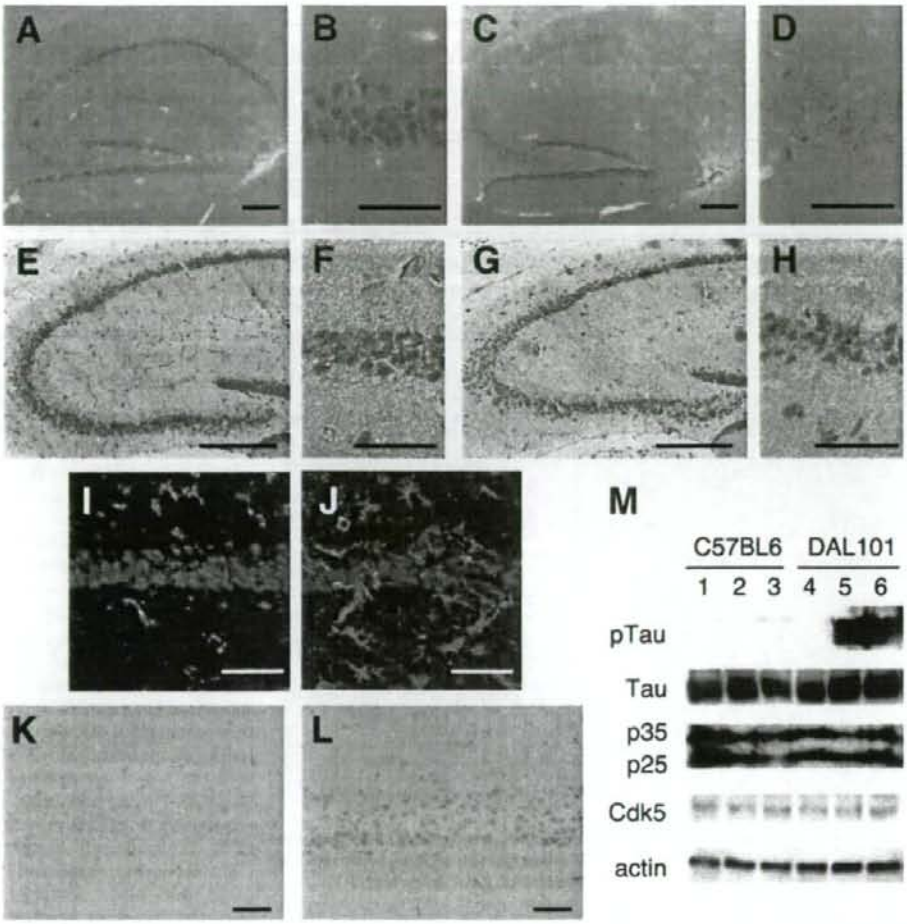

Figure 4. Hippocampal degeneration in DAL mice. ***A***, ***B***, ***K***, Twelve-month-old C57BL/6. ***E***, ***F***, ***I***, Eighteen-month-old C57BL/6. ***C***, ***D***, ***L***, Twelve-month-old DAL101. ***G***, ***H***, ***J***, Eighteen-month-old DAL101. ***A***, ***C***, Hippocampus was stained with H&E. Scale bar, 200 μm. ***B***, ***D***, The CA1 region stained with H&E was expanded. Scale bar, 50 μm. ***E***, ***G***, Hippocampus was stained with the antibody to NeuN. Scale bar, 250 μm. ***F***, ***H***, The CA1 region stained with the antibody to NeuN was expanded. Scale bar, 50 μm. ***I***, ***J***, The CA1 region was stained with antibodies to GFAP (green) and NeuN (red). Scale bar, 50 μm. ***K***, ***L***, The CA1 region was stained with anti-phosphorylated tau antibody (AT8). Scale bar, 50 μm. ***M***, Representative immunoblots of hippocampal lysates from 18-month-old C57BL/6 (lanes 1–3) and DAL101 (lanes 4–6) mice probed with antibodies to phosphorylated tau (pTau), pan-tau (Tau), Cdk5 activator proteins (p25 and p35), Cdk5, and actin.

Table 1. Number of neurons in the hippocampus of C57BL/6 and DAL101 mice

	C57BL/6	DAL101	*p*
Old	$n = 6$	$n = 8$	
CA1 (no./mm^2)	2172.01 ± 259.76	1593.00 ± 356.38	0.0057
Hilus (no./mm^2)	591.67 ± 88.86	462.50 ± 84.98	0.0172
Young	$n = 5$	$n = 4$	
CA1 (no./mm^2)	2023.20 ± 218.47	2083.50 ± 197.39	0.6810
Hilus (no./mm^2)	434.00 ± 44.50	427.50 ± 67.02	0.8658

The brain sections of old (1–1.5 years of age) and young (0.5 year of age) mice were stained with H&E, and the total numbers of neurons in area CA1 and hilus of the dentate gyrus were counted. Data are presented as mean ± SD.

object approximately an equal number of times during the training period (Fig. 6*A*), indicating comparable attention, motivation, and visual perception. One day after training, one of the conditioned objects was replaced with a novel object (cubic, c). During 5 min of testing, young C57BL/6 (6 months of age) and DAL101 (6–8 months of age) mice and aged C57BL/6 (12 months of age) mice, but not aged DAL101 (11–14 months of age), DAL102 (12 months of age), and DAL103 (12 months of age) mice, approached or sniffed the novel object more times than the original object (Fig. 6*B*). These results indicated that aged DAL101 showed a deficit in visual recognition memory, whereas young DAL101 and aged CTL mice showed intact ability to detect a novel object. This age-dependent deficit in recognition memory agrees with the histological neuronal degeneration described above. Similar disability was observed in other lines of aged DAL mice (DAL102 and DAL103), indicating that the memory deficit was not specific to aged DAL101.

To examine more carefully whether ALDH2 deficiency affects cognitive impairment, DAL101 was tested in the Morris water

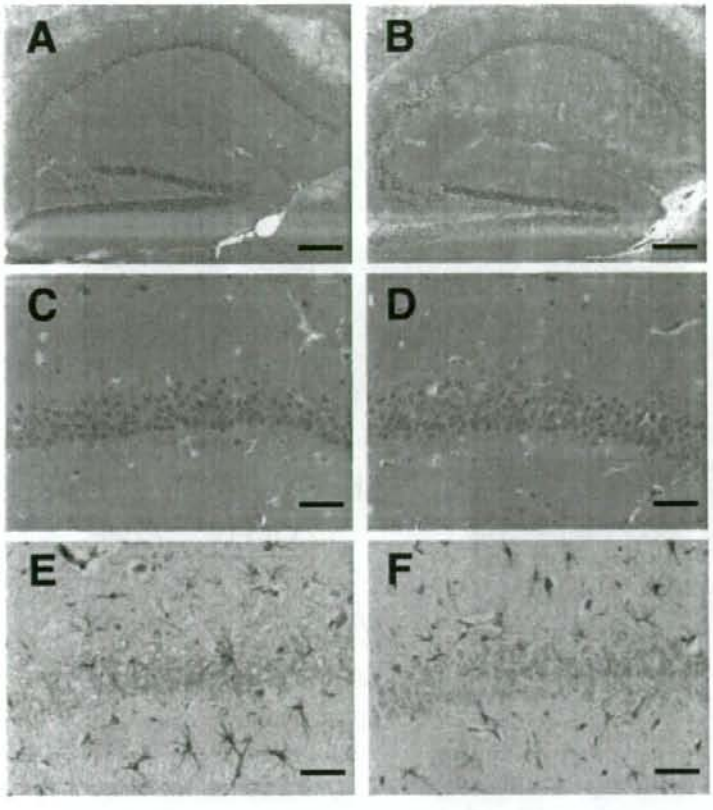

Figure 5. No obvious hippocampal degeneration was observed in the hippocampus in young DAL mice. ***A***, ***B***, Hippocampus was stained with H&E. Scale bar, 200 μm. ***C***, ***D***, The CA1 region stained with H&E was expanded. Scale bar, 50 μm. ***E***, ***F***, The CA1 region was stained with anti-GFAP antibody. Scale bar, 50 μm. ***A***, ***C***, ***E***, Six-month-old C57BL/6. ***B***, ***D***, ***F***, Six-month-old DAL101.

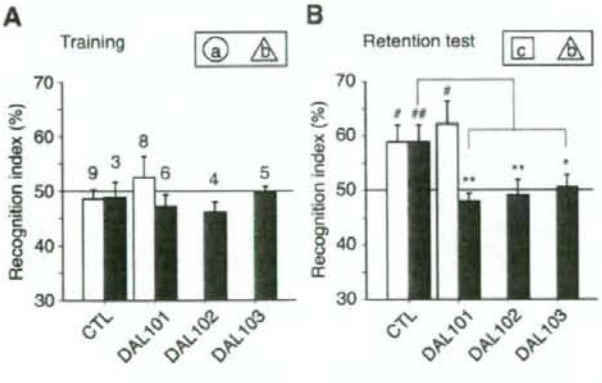

Figure 6. Decreased object recognition memory in aged DAL mice. ALDH2 deficiency impaired memory for object recognition. ***A***, Training for visible object recognition. During 10 min of training, two objects (a and b) were presented to a mouse. C57BL/6 mice, which were used as a control (CTL), and all DAL mice had equal preferences for two objects, a and b. Filled bars, Aged mice; open bars, young mice (see Materials and Methods). The numbers on the bars indicate the number of animals examined. ***B***, Testing for novel object recognition. During 5 min of testing, one of the conditioned objects was replaced by a novel object (c). Young mice and aged CTL mice, but not aged DAL mice, showed recognition memory 1 d after a training session. $^{\#}p < 0.05$, $^{\#\#}p < 0.01$ versus index in a training session; $^{*}p < 0.05$, $^{**}p < 0.01$.

maze (MWM), a hippocampus-dependent paradigm used to assess the ability to acquire, process, and recall spatial information by using escape latency as an indicator of learning (D'Hooge and De Deyn, 2001). Because of the physical demands of this study, only female mice were used. At 6 months of age, no obvious pathology was apparent in any brain region of DAL mice (Fig. 5, Table 1). Nevertheless, analysis of cognitive function at this age is of great importance to evaluate whether mice are born with learning and memory impairment or whether they develop cognitive deficit in an age-dependent manner. We found that, at 6 months of age, DAL mice had intact spatial learning and memory, and no deficits in probe trials (Fig. 7*A*,*B*). They required 3 d of training to reach criterion (escape latency of <20 s) and spent significantly more time over the trained quadrant compared with other quadrants during probe trials. No obvious difference between DAL and CTL mice was observed. These results indicated that DAL mice were born normally and did not develop cognitive deficit during young adulthood.

At 1 and 1.5 year of age, DAL mice were still able to learn the MWM task; however, they required 5 d of training to reach criterion (escape latency of <20 s) compared with the 3 d of age-matched CTL mice (Fig. 7*A*). Furthermore, time spent in the target quadrant of DAL mice during probe trials was significantly shorter than that of CTL mice and not significantly more compared with other nontarget quadrants (Fig. 7*B*). To assess whether the spatial learning and memory deficits observed in DAL mice were attributable to deficient escape motivation or impairment of visual and/or motor performance, the visible platform was used. Escape latencies after the training in this experiment were not different between DAL and CTL mice (Fig. 7*C*). Swimming speeds were also determined to exclude the possibility of different swimming abilities. No significant difference in speeds between DAL and CTL mice was observed, whereas speeds decreased age-dependently (Fig. 7*D*), suggesting that sensorimotor disturbances were not differentially affecting their performance.

Cognitive impairments in DAL mice are accelerated by APOE-knock-out

We reported previously that the *ALDH2*2* allele is a synergistic risk for AD with ε4 allele of the apolipoprotein E gene (Kamino et al., 2000). We then sought to examine whether apoE affect phenotypes of

DAL mice and examined DAL mice without apoE (DAL/$ApoE^{-/-}$) at 6 months of age in the MWM. They were not able to learn the MWM task, whereas both DAL and $ApoE^{-/-}$ mice required only 3 d of training to reach criterion (escape latency of <20 s) (Fig. 8*A*). Furthermore, time spent in the target quadrant of DAL/$ApoE^{-/-}$ mice during probe trials was significantly shorter than that of both DAL and $ApoE^{-/-}$ mice (Fig. 8*B*). Escape latencies after training using the visible platform were not different among DAL/$ApoE^{-/-}$, DAL, and $ApoE^{-/-}$ mice (Fig. 8*C*), suggesting that sensorimotor disturbances were not differentially affecting their performance. Thus, these results indicate that the ApoE depletion enhances the learning and memory deficits of DAL mice.

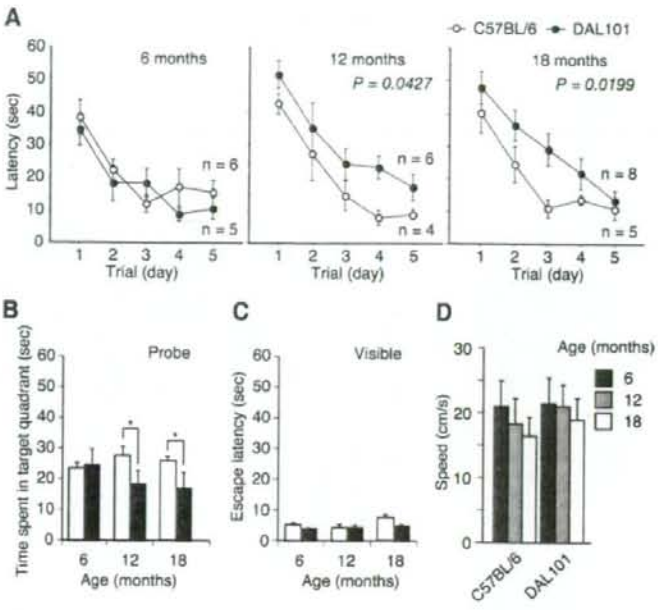

Figure 7. Age-dependent onset of cognitive impairment in DAL mice. Performance on the MWM test. ***A***, At the age of 6 months, time to reach a hidden platform (latency) was similar in the DAL101 and C57BL/6 mice. However, the 12- and 18-month-old DAL101 mice showed profound impairment compared with C57BL/6 mice. ***B***, Probe test performed 1 h after the hidden platform acquisition period. At the age of 6 months, time spent in the target quadrant was similar in the DAL101 (filled bars) and C57BL/6 (open bars) mice. However, the 12- and 18-month-old DAL101 mice spent a shorter time searching in the target quadrant than C57BL/6 mice (mean ± SD). *$p < 0.05$. ***C***, Time to reach visible platform locations. Filled bars, DAL101; open bars, C57BL/6. ***D***, Swimming speed during probe trial.

Discussion

We reported here that transgenic mice expressing a mouse version of dominant-negative ALDH2 showed enhanced accumulation of ROS end products and age-dependent learning and memory deficits. ALDH enzymes efficiently oxidize HNE, a highly toxic product of lipid peroxidation (Ohta et al., 2004; Vasiliou et al., 2004). Interestingly, mitochondria ALDH2 metabolize nitroglycerin, which has been used for over a century in the therapy of cardiovascular disease (Chen et al., 2002). Nitroglycerin tolerance developed by chronic therapy is associated with a decrease in ALDH2 activity and an increase of ROS (Chen and Stamler, 2006), and, at that time, ALDH2 itself is inactivated by various oxidants (Wenzel et al., 2007). However, ALDH2 activity was found to increase in liver with age and in the brain of AD patients (Picklo et al., 2001; Yoon et al., 2006), suggesting that sufficient amount of active ADLH2 is needed to detoxify the increased HNE that occurs in aging and neurodegenerative diseases.

The construction of model animals by genetic manipulation is one of the best methods to analyze the involvement of particular genes in the defense against oxidative stress at the animal level. In mice defective in Mn-superoxide dismutase (SOD), oxidative stress accumulated, and mitochondrial dysfunction and subsequent cell death were observed (Melov et al., 1998). Because the model mice died during the first few postnatal weeks, their pathology was too severe to investigate age-dependent degeneration. Furthermore, mice defective in phospholipid hydroperoxide glutathione peroxidase (PHGPx) were embryonic lethal (Imai et al., 2003). PHGPx is the only known enzyme that directly reduces lipid hydroperoxide; however, knock-out mice deficient in Cu, Zn-SOD, cellular glutathione peroxidase, and catalase developed normally and showed no marked pathological changes under normal physiological conditions (Reaume et al., 1996; Esposito et al., 2000; Ho et al., 2004), indicating that their defects in major antioxidant defense mechanisms are strongly compensated by each other. In the case of DAL mice, no obvious pathological features, including cognitive function, were observed in young mice (6 months of age), indicating that no physiological and neurological changes would occur during their growth and development. After maturation, oxidative stress accumulated in the brain and cognitive deficits developed in aged DAL mice. The importance of this model mouse is the age-dependent onset of neurodegenerative disorders, which will be helpful for understanding human disease.

ALDH belongs to a large family consisting of at least 16 different genes in humans, and are involved in the metabolic systems of various alcohols and aldehydes according to their distribution and substrate specificity (Vasiliou and Nebert, 2005). It is likely that knocking out one such gene causes moderate change in aldehyde metabolism, because the knocked-out enzyme would be complemented with other members of the gene family. In fact, in ALDH2 knock-out mice, methoxyacetaldehyde metabolism is markedly reduced in liver, but no apparent abnormality was observed (Kitagawa et al., 2000). This discrepancy suggests that the phenotype observed in DAL mice is not simply attributable to the decrease in the ALDH2 activity. ALDH2*2 may inactivate not only ALDH2 but also the other member, such as ALDH5A, of the ALDH family presumably by forming heterotetramers. In humans, however, the suppression of ALDH2 activity by ALDH2*2 causes various disorders, presumably because of increased oxidative stress. For instance, ALDH2 deficiency was found to contribute to the risk of complication with diabetes mellitus, hypertension, myocardial infarction, osteoporosis, and cancer (Suzuki et al., 1996; Amamoto et al., 2002; Takagi et al., 2002; Yokoyama and Omori, 2003; Yamaguchi et al., 2006). Therefore, we expected the development of model animals closer to humans by introducing the *ALDH2*2* gene. The resultant DAL mice showed

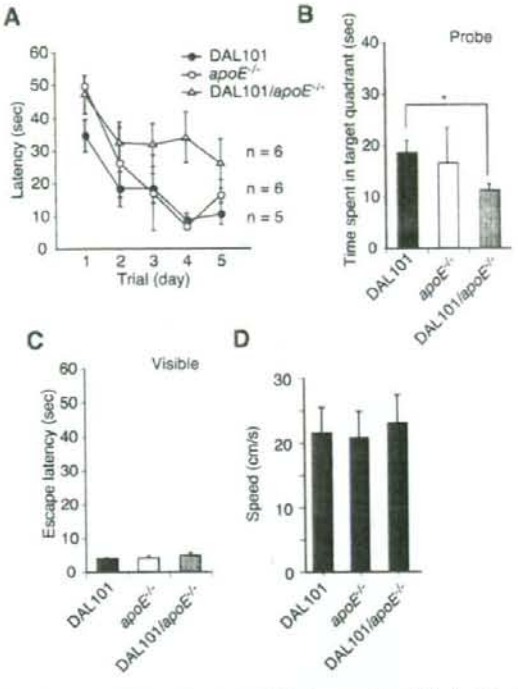

Figure 8. Onset of cognitive impairment in DAL mice was enhanced by lacking in ApoE. Performance on the MWM test. ***A***, At the age of 6 months, DAL101 mice in the absence of ApoE (DAL101/*ApoE*$^{-/-}$) showed profound impairment compared with DAL101 and *ApoE*$^{-/-}$ mice. $p < 0.05$ against DAL101 and *ApoE*$^{-/-}$ mice, respectively. ***B***, Probe test performed 1 h after the hidden platform acquisition period. DAL101/*ApoE*$^{-/-}$ spent a shorter time searching in the target quadrant than DAL101 and *ApoE*$^{-/-}$ mice (mean ± SD). *$p < 0.05$. ***C***, Time to reach visible platform locations. ***D***, Swimming speed during probe trial.

accumulated oxidative stress and their lifespan decreased (Fig. 3). Aging is associated with changes in physiological characteristics, including muscle weakness and hair decolorization, and many physiological functions. The causes, however, are multifactorial and several studies have suggested that oxidative stress plays an important role. ALDH2 could reduce oxidative stress in multiple organs. Indeed, we have observed amytrophy developed in muscles of Tg-mice expressing ALDH2*2 (I. Ohsawa, K. Nishimaki, Y. Suzuki, T. Nukina, E. Kodaira, M. Sano, S. Yamaguchi, S. Yagihashi, and S. Ohta, unpublished observation). The molecular mechanisms that trigger dementia symptoms have been highly elusive; however, marked increases in oxidative stress, typically represented by HNE, were reported in the hippocampus and superior and middle temporal gyrus of patients with mild cognitive impairment and in those with early AD compared with age-matched healthy individuals (Williams et al., 2006). These results, which are in agreement with the results of LPO analysis in CSF (Pratico et al., 2002), suggest that oxidative stress, typically represented by HNE, is involved in the causes of the onset of dementia. As shown in Figure 3*A*, age-dependent accumulation of HNE in the brain of DAL mice was observed and the ALDH2-defective hippocampal and cortical neurons were highly susceptible to HNE (Fig. 2). These findings suggest that earlier accumulation of HNE in the ALDH2-deficient brain is responsible for a trigger of cognitive decline.

The accumulation of aldehydes, including HNE, not only induces neuronal death but also causes synaptic dysfunction because of mechanisms such as reducing Na^+,K^+-ATPase activity (Pedersen et al., 1999) and markedly inhibits microtubule formation and neurite outgrowth (Neely et al., 1999). Furthermore, there have been a number of reports on the relationship between neurofibrillary tangle (NFT) and oxidative stress (Zarkovic, 2003). Positive immunohistochemical staining of the DAL mouse brain with phosphorylation-specific monoclonal antibody against tau (Fig. 4*L*) suggested that the accumulation of HNE induced by ALDH2 deficiency causes age-dependent tau hyperphosphorylation, which is a pathological feature characteristic of AD. It has been further reported that HNE induces structural changes in phosphorylated tau by its modification of it and formation of NFT-like tau assemblies *in vitro* (Takeda et al., 2000; Liu et al., 2005). Cdk5 is thought to be responsible for hyperphosphorylation of tau in AD and activated by p35, which may be cleaved to more stable fragment p25 (Cruz and Tsai, 2004). However, although some experiments using animals overexpressing Cdk5, p35, or p25 have supported a causal relationship between Cdk5/p25 and NFT, there is still discrepancy among studies. As shown in Figure 4*M*, no obvious change of their expression level was observed, whereas tau was hyperphosphorylated in the hippocampus of old DAL mice. Thus, p35/p25 may be not essential for the tau hyperphosphorylation in DAL mice.

To examine the effects of ALDH2 deficiency on memory, we used two tests, vORT and MWM. In both tests, the form of memory depends on the hippocampus. Aged DAL mice showed a deficit in both visual recognition memory and spatial learning and memory, whereas young DAL mice showed intact ability to form these memories (Figs. 6, 7). This age-related deficit in memory agrees with histological neuronal degeneration in the hippocampus of aged DAL mice (Fig. 4). We observed a similar disability of recognition memory in three independent lines of aged DAL mice (DAL101, DAL102, and DAL103), indicating that the expression of ALDH2*2 in the brain is sufficient to induce deficit in hippocampal-dependent learning and memory.

We found that the deletion of ApoE enhances learning and memory deficits of DAL mice (Fig. 8). The strength of binding between human APOE and HNE was $\varepsilon 2 > \varepsilon 3 > \varepsilon 4$, which was in agreement with the preventive activity of APOE against cell death caused by HNE (Pedersen et al., 2000). Thus, APOE eliminates free HNE and the possession of APOE-$\varepsilon 4$, the APOE with the weakest HNE elimination ability, leading to the accumulation of HNE in neurons and increasing oxidative stress. These results agree with our previous epidemiological investigation (Kamino et al., 2000), in which *ALDH2*2* and *APOE-ε4* alleles synergistically increased the risk of AD. Together, the accumulation of HNE in ALDH2-deficient mice is further intensified by the loss of ApoE. However, no obvious neurodegeneration, activation of astrocyte, nor hyperphosphorylation of the tau protein was apparent in any brain region of DAL/*ApoE*$^{-/-}$ mice at 6 months of age. Thus, additional investigations will be required to clarify cellular and molecular mechanisms of cognitive impairments in these mice.

Because highly toxic aldehydes are generated spontaneously by lipid peroxidation, there are a variety of mechanisms for their detoxification including binding with glutathione and reduction by aldose reductase, ADH and ABAD. Also, multiple ALDHs are considered to oxidize aldehydes. It is quite interesting that mitochondrial ALDH5A as well as ALDH2 plays an important role in the detoxification of HNE in the CNS (Murphy et al., 2003). In this study, we established transgenic mice with reduced ALDH2 activity and found that age-dependent neurodegeneration ac-

companying memory loss was caused by the introduction of a single mutant gene. This study emphasizes that the contribution of toxic analdehyde(s) derived from oxidative stress is sufficient to develop age-dependent neurodegeneration with memory loss.

References

Amamoto K, Okamura T, Tamaki S, Kita Y, Tsujita Y, Kadowaki T, Nakamura Y, Ueshima H (2002) Epidemiologic study of the association of low-Km mitochondrial acetaldehyde dehydrogenase genotypes with blood pressure level and the prevalence of hypertension in a general population. Hypertens Res 25:857–864.

Biernat J, Mandelkow EM, Schröter C, Lichtenberg-Kraag B, Steiner B, Berling B, Meyer H, Mercken M, Vandermeeren A, Goedert M, Mandelkow E (1992) The switch of tau protein to an Alzheimer-like state includes the phosphorylation of two serine-proline motifs upstream of the microtubule binding region. EMBO J 11:1593–1597.

Bosron WF, Li TK (1986) Genetic polymorphism of human liver alcohol and aldehyde dehydrogenases, and their relationship to alcohol metabolism and alcoholism. Hepatology 6:502–510.

Chen Z, Stamler JS (2006) Bioactivation of nitroglycerin by the mitochondrial aldehyde dehydrogenase. Trends Cardiovasc Med 16:259–265.

Chen Z, Zhang J, Stamler JS (2002) Identification of the enzymatic mechanism of nitroglycerin bioactivation. Proc Natl Acad Sci USA 99:8306–8311.

Cruz JC, Tsai LH (2004) A Jekyll and Hyde kinase: roles for Cdk5 in brain development and disease. Curr Opin Neurobiol 14:390–394.

D'Hooge R, De Deyn PP (2001) Applications of the Morris water maze in the study of learning and memory. Brain Res Brain Res Rev 36:60–90.

Esposito LA, Kokoszka JE, Waymire KG, Cottrell B, MacGregor GR, Wallace DC (2000) Mitochondrial oxidative stress in mice lacking the glutathione peroxidase-1 gene. Free Radic Biol Med 28:754–766.

Gadoni E, Olivero A, Miglietta A, Bocca C, Gabriel L (1993) Cytoskeletal modifications induced by 4-hydroxynonenal. Cytotechnology 11 [Suppl 1]:S62–S64.

Hamann M, Meisler MH, Richter A (2003) Motor disturbances in mice with deficiency of the sodium channel gene Scn8a show features of human dystonia. Exp Neurol 184:830–838.

Higuchi S, Matsushita S, Masaki T, Yokoyama A, Kimura M, Suzuki G, Mochizuki H (2004) Influence of genetic variations of ethanol-metabolizing enzymes on phenotypes of alcohol-related disorders. Ann NY Acad Sci 1025:472–480.

Ho YS, Xiong Y, Ma W, Spector A, Ho DS (2004) Mice lacking catalase develop normally but show differential sensitivity to oxidant tissue injury. J Biol Chem 279:32804–32812.

Imai H, Hirao F, Sakamoto T, Sekine K, Mizukura Y, Saito M, Kitamoto T, Hayasaka M, Hanaoka K, Nakagawa Y (2003) Early embryonic lethality caused by targeted disruption of the mouse PHGPx gene. Biochem Biophys Res Commun 305:278–286.

Isacson O, Fischer W, Wictorin K, Dawbarn D, Björklund A (1987) Astroglial response in the excitotoxically lesioned neostriatum and its projection areas in the rat. Neuroscience 20:1043–1056.

Jo SA, Kim E, Han C, Park MH, Jo I (2007) P-166A Glu487Lys polymorphism in the gene for mitochondrial aldehyde dehydrogenase 2 is associated with mild cognitive impairment in elderly Korean men. Alzheimers Dement 3:S151.

Kamino K, Nagasaka K, Imagawa M, Yamamoto H, Yoneda H, Ueki A, Kitamura S, Namekata K, Miki T, Ohta S (2000) Deficiency in mitochondrial aldehyde dehydrogenase increases the risk for late-onset Alzheimer's disease in the Japanese population. Biochem Biophys Res Commun 273:192–196.

Kim KS, Lee KW, Lee KW, Im JY, Yoo JY, Kim SW, Lee JK, Nestler EJ, Han PL (2006) Adenylyl cyclase type 5 (AC5) is an essential mediator of morphine action. Proc Natl Acad Sci USA 103:3908–3913.

Kitagawa K, Kawamoto T, Kunugita N, Tsukiyama T, Okamoto K, Yoshida A, Nakayama K, Nakayama K (2000) Aldehyde dehydrogenase (ALDH) 2 associates with oxidation of methoxyacetaldehyde; in vitro analysis with liver subcellular fraction derived from human and Aldh2 gene targeting mouse. FEBS Lett 476:306–311.

Liou YC, Sun A, Ryo A, Zhou XZ, Yu ZX, Huang HK, Uchida T, Bronson R, Bing G, Li X, Hunter T, Lu KP (2003) Role of the prolyl isomerase Pin1 in protecting against age-dependent neurodegeneration. Nature 424:556–561.

Liu Q, Smith MA, Aváil J, DeBernardis J, Kansal M, Takeda A, Zhu X, Nunomura A, Honda K, Moreira PI, Oliveira CR, Santos MS, Shimohama S, Aliev G, de la Torre J, Ghanbari HA, Siedlak SL, Harris PL, Sayre LM, Perry G (2005) Alzheimer-specific epitopes of tau represent lipid peroxidation-induced conformations. Free Radic Biol Med 38:746–754.

Lovell MA, Ehmann WD, Mattson MP, Markesbery WR (1997) Elevated 4-hydroxynonenal in ventricular fluid in Alzheimer's disease. Neurobiol Aging 18:457–461.

Mark RJ, Pang Z, Geddes JW, Uchida K, Mattson MP (1997) Amyloid β-peptide impairs glucose transport in hippocampal and cortical neurons: involvement of membrane lipid peroxidation. J Neurosci 17:1046–1054.

Mattson MP (2004) Pathways towards and away from Alzheimer's disease. Nature 430:631–639.

Melov S, Schneider JA, Day BJ, Hinerfeld D, Coskun P, Mirra SS, Crapo JD, Wallace DC (1998) A novel neurological phenotype in mice lacking mitochondrial manganese superoxide dismutase. Nat Genet 18:159–163.

Miyakawa T, Yared E, Pak JH, Huang FL, Huang KP, Crawley JN (2001) Neurogranin null mutant mice display performance deficits on spatial learning tasks with anxiety related components. Hippocampus 11:763–775.

Miyamoto Y, Chen L, Sato M, Sokabe M, Nabeshima T, Pawson T, Sakai R, Mori N (2005) Hippocampal synaptic modulation by the phosphotyrosine adapter protein ShcC/N-Shc via interaction with the NMDA receptor. J Neurosci 25:1826–1835.

Mizushima S, Nagata S (1990) pEF-BOS, a powerful mammalian expression vector. Nucleic Acids Res 18:5322.

Montine KS, Olson SJ, Amarnath V, Whetsell Jr WO, Graham DG, Montine TJ (1997) Immunohistochemical detection of 4-hydroxy-2-nonenal adducts in Alzheimer's disease is associated with inheritance of APOE4. Am J Pathol 150:437–443.

Murakami Y, Ohsawa I, Kasahara T, Ohta S (2008) Cytoprotective role of mitochondrial amyloid beta peptide-binding alcohol dehydrogenase against a cytotoxic aldehyde. Neurobiol Aging, in press.

Murphy TC, Amarnath V, Gibson KM, Picklo Sr MJ (2003) Oxidation of 4-hydroxy-2-nonenal by succinic semialdehyde dehydrogenase (ALDH5A). J Neurochem 86:298–305.

Murray IV, Liu L, Komatsu H, Uryu K, Xiao G, Lawson JA, Axelsen PH (2007) Membrane-mediated amyloidogenesis and the promotion of oxidative lipid damage by amyloid beta proteins. J Biol Chem 282:9335–9345.

Neely MD, Sidell KR, Graham DG, Montine TJ (1999) The lipid peroxidation product 4-hydroxynonenal inhibits neurite outgrowth, disrupts neuronal microtubules, and modifies cellular tubulin. J Neurochem 72:2323–2333.

Ohsawa I, Nishimaki K, Yasuda C, Kamino K, Ohta S (2003a) Deficiency in a mitochondrial aldehyde dehydrogenase increases vulnerability to oxidative stress in PC12 cells. J Neurochem 84:1110–1117.

Ohsawa I, Kamino K, Nagasaka K, Ando F, Niino N, Shimokata H, Ohta S (2003b) Genetic deficiency of a mitochondrial aldehyde dehydrogenase increases serum lipid peroxides in community-dwelling females. J Hum Genet 48:404–409.

Ohsawa I, Ishikawa M, Takahashi K, Watanabe M, Nishimaki K, Yamagata K, Katsura K, Katayama Y, Asoh S, Ohta S (2007) Hydrogen acts as a therapeutic antioxidant by selectively reducing cytotoxic oxygen radicals. Nat Med 13:688–694.

Ohta S, Ohsawa I, Kamino K, Ando F, Shimokata H (2004) Mitochondrial ALDH2 deficiency as an oxidative stress. Ann NY Acad Sci 1011:36–44.

Pedersen WA, Cashman NR, Mattson MP (1999) The lipid peroxidation product 4-hydroxynonenal impairs glutamate and glucose transport and choline acetyltransferase activity in NSC-19 motor neuron cells. Exp Neurol 155:1–10.

Pedersen WA, Chan SL, Mattson MP (2000) A mechanism for the neuroprotective effect of apolipoprotein E: isoform-specific modification by the lipid peroxidation product 4-hydroxynonenal. J Neurochem 74:1426–1433.

Picklo MJ, Olson SJ, Markesbery WR, Montine TJ (2001) Expression and activities of aldo-keto oxidoreductases in Alzheimer disease. J Neuropathol Exp Neurol 60:686–695.

Praticò D, Clark CM, Liun F, Rokach J, Lee VY, Trojanowski JQ (2002) Increase of brain oxidative stress in mild cognitive impairment: a possible predictor of Alzheimer disease. Arch Neurol 59:972–976.

Reagan LP, Magariños AM, Yee DK, Swzeda LI, Van Bueren A, McCall AL, McEwen BS (2000) Oxidative stress and HNE conjugation of GLUT3 are increased in the hippocampus of diabetic rats subjected to stress. Brain Res 862:292–300.

Reaume AG, Elliott JL, Hoffman EK, Kowall NW, Ferrante RJ, Siwek DF, Wilcox HM, Flood DG, Beal MF, Brown Jr RH, Scott RW, Snider WD (1996) Motor neurons in Cu/Zn superoxide dismutase-deficient mice develop normally but exhibit enhanced cell death after axonal injury. Nat Genet 13:43–47.

Sayre LM, Zelasko DA, Harris PL, Perry G, Salomon RG, Smith MA (1997) 4-Hydroxynonenal-derived advanced lipid peroxidation end products are increased in Alzheimer's disease. J Neurochem 68:2092–2097.

Schneider C, Tallman KA, Porter NA, Brash AR (2001) Two distinct pathways of formation of 4-hydroxynonenal. Mechanisms of nonenzymatic transformation of the 9- and 13-hydroperoxides of linoleic acid to 4-hydroxyalkenals. J Biol Chem 276:20831–20838.

Siems W, Grune T (2003) Intracellular metabolism of 4-hydroxynonenal. Mol Aspects Med 24:167–175.

Srivastava S, Chandra A, Ansari NH, Srivastava SK, Bhatnagar A (1998) Identification of cardiac oxidoreductase(s) involved in the metabolism of the lipid peroxidation-derived aldehyde-4-hydroxynonenal. Biochem J 329:469–475.

Suzuki Y, Muramatsu T, Taniyama M, Atsumi Y, Suematsu M, Kawaguchi R, Higuchi S, Asahina T, Murata C, Handa M, Matsuoka K (1996) Mitochondrial aldehyde dehydrogenase in diabetes associated with mitochondrial tRNA(Leu(UUR)) mutation at position 3243. Diabetes Care 19:1423–1425.

Takagi S, Iwai N, Yamauchi R, Kojima S, Yasuno S, Baba T, Terashima M, Tsutsumi Y, Suzuki S, Morii I, Hanai S, Ono K, Baba S, Tomoike H, Kawamura A, Miyazaki S, Nonogi H, Goto Y (2002) Aldehyde dehydrogenase 2 gene is a risk factor for myocardial infarction in Japanese men. Hypertens Res 25:677–681.

Takashima A (2006) GSK-3 is essential in the pathogenesis of Alzheimer's disease. J Alzheimers Dis 9:309–317.

Takeda A, Smith MA, Avilá J, Nunomura A, Siedlak SL, Zhu X, Perry G, Sayre LM (2000) In Alzheimer's disease, heme oxygenase is coincident with Alz50, an epitope of tau induced by 4-hydroxy-2-nonenal modification. J Neurochem 75:1234–1241.

Tang FR, Chia SC, Zhang S, Chen PM, Gao H, Liu CP, Khanna S, Lee WL (2005) Glutamate receptor 1-immunopositive neurons in the gliotic CA1 area of the mouse hippocampus after pilocarpine-induced status epilepticus. Eur J Neurosci 21:2361–2374.

Tjalkens RB, Cook LW, Petersen DR (1999) Formation and export of the glutathione conjugate of 4-hydroxy-2,3-*E*-nonenal (4-HNE) in hepatoma cells. Arch Biochem Biophys 361:113–119.

Uchida K (2003) 4-Hydroxy-2-nonenal: a product and mediator of oxidative stress. Prog Lipid Res 42:318–343.

Vasiliou V, Nebert DW (2005) Analysis and update of the human aldehyde dehydrogenase (ALDH) gene family. Hum Genomics 2:138–143.

Vasiliou V, Pappa A, Estey T (2004) Role of human aldehyde dehydrogenases in endobiotic and xenobiotic metabolism. Drug Metab Rev 36:279–299.

Wakabayashi-Ito N, Nagata S (1994) Characterization of the regulatory elements in the promoter of the human elongation factor-1 alpha gene. J Biol Chem 269:29831–29837.

Wang B, Wang J, Zhou S, Tan S, He X, Yang Z, Xie YC, Li S, Zheng C, Ma X (2008) The association of mitochondrial aldehyde dehydrogenase gene (ALDH2) polymorphism with susceptibility to late-onset Alzheimer's disease in Chinese. J Neurol Sci 268:172–175.

Wang H, Ferguson GD, Pineda VV, Cundiff PE, Storm DR (2004) Overexpression of type-1 adenylyl cyclase in mouse forebrain enhances recognition memory and LTP. Nat Neurosci 7:635–642.

Wenzel P, Hink U, Oelze M, Schuppan S, Schaeuble K, Schildknecht S, Ho KK, Weiner H, Bachschmid M, Munzel T, Daiber A (2007) Role of reduced lipoic acid in the redox regulation of mitochondrial aldehyde dehydrogenase (ALDH-2) activity. Implications for mitochondrial oxidative stress and nitrate tolerance. J Biol Chem 282:792–799.

Williams TI, Lynn BC, Markesbery WR, Lovell MA (2006) Increased levels of 4-hydroxynonenal and acrolein, neurotoxic markers of lipid peroxidation, in the brain in Mild Cognitive Impairment and early Alzheimer's disease. Neurobiol Aging 27:1094–1099.

Xie C, Lovell MA, Markesbery WR (1998) Glutathione transferase protects neuronal cultures against four hydroxynonenal toxicity. Free Radic Biol Med 25:979–988.

Yamaguchi J, Hasegawa Y, Kawasaki M, Masui T, Kanoh T, Ishiguro N, Hamajima N (2006) ALDH2 polymorphisms and bone mineral density in an elderly Japanese population. Osteoporos Int 17:908–913.

Yokoyama A, Omori T (2003) Genetic polymorphisms of alcohol and aldehyde dehydrogenases and risk for esophageal and head and neck cancers. Jpn J Clin Oncol 33:111–121.

Yoon M, Madden MC, Barton HA (2006) Developmental expression of aldehyde dehydrogenase in rat: a comparison of liver and lung development. Toxicol Sci 89:386–398.

Yoritaka A, Hattori N, Uchida K, Tanaka M, Stadtman ER, Mizuno Y (1996) Immunohistochemical detection of 4-hydroxynonenal protein adducts in Parkinson disease. Proc Natl Acad Sci USA 93:2696–2701.

Zarkovic K (2003) 4-Hydroxynonenal and neurodegenerative diseases. Mol Aspects Med 24:293–303.

Biochemical and Biophysical Research Communications 373 (2008) 30–35

Contents lists available at ScienceDirect

Biochemical and Biophysical Research Communications

journal homepage: www.elsevier.com/locate/ybbrc

Inhalation of hydrogen gas reduces infarct size in the rat model of myocardial ischemia–reperfusion injury

Kentaro Hayashida [b], Motoaki Sano [a,d,*], Ikuroh Ohsawa [e,f], Ken Shinmura [c], Kayoko Tamaki [c], Kensuke Kimura [b], Jin Endo [b], Takaharu Katayama [b], Akio Kawamura [b], Shun Kohsaka [b], Shinji Makino [a], Shigeo Ohta [e], Satoshi Ogawa [b], Keiichi Fukuda [a]

[a] Department of Regenerative Medicine and Advanced Cardiac Therapeutics, Keio University School of Medicine, 35 Shinanomachi Shinjuku-ku, Tokyo 160-8582, Japan
[b] Division of Cardiology, Keio University School of Medicine, Tokyo 160-8582, Japan
[c] Division of Geriatric Medicine, Department of Internal Medicine, Keio University School of Medicine, Tokyo 160-8582, Japan
[d] Precursory Research for Embryonic Science and Technology (PRESTO), Japan Science and Technology Agency, Saitama 332-0012, Japan
[e] Department of Biochemistry and Cell Biology, Institute of Development and Aging Science, Graduate School of Medicine, Nippon Medical School, Kawasaki city 211-8533, Japan
[f] Department of Biochemistry and Cell Biology, The Center of Molecular Hydrogen Medicine, Institute of Development and Aging Science, Graduate School of Medicine, Nippon Medical School, Kawasaki city 211-8533, Japan

ARTICLE INFO

Article history:
Received 19 May 2008
Available online 9 June 2008

Keywords:
Ischemia–reperfusion injury
Anti-oxidant
Myocardial infarction
H_2

ABSTRACT

Inhalation of hydrogen (H_2) gas has been demonstrated to limit the infarct volume of brain and liver by reducing ischemia–reperfusion injury in rodents. When translated into clinical practice, this therapy must be most frequently applied in the treatment of patients with acute myocardial infarction, since angioplastic recanalization of infarct-related occluded coronary artery is routinely performed. Therefore, we investigate whether H_2 gas confers cardioprotection against ischemia–reperfusion injury in rats. In isolated perfused hearts, H_2 gas enhances the recovery of left ventricular function following anoxia-reoxygenation. Inhaled H_2 gas is rapidly transported and can reach 'at risk' ischemic myocardium before coronary blood flow of the occluded infarct-related artery is reestablished. Inhalation of H_2 gas at incombustible levels during ischemia and reperfusion reduces infarct size without altering hemodynamic parameters, thereby preventing deleterious left ventricular remodeling. Thus, inhalation of H_2 gas is promising strategy to alleviate ischemia–reperfusion injury coincident with recanalization of coronary artery.

Acute myocardial infarction is a leading cause of death worldwide. Reduction of infarct size is an important therapeutic goal, since the size of the infarct is directly linked to short-term and long-term morbidity and mortality [1]. The prognosis of acute myocardial infarction has been improved dramatically with the development of highly successful approaches to restore blood flow by primary percutaneous coronary intervention (PCI) to the ischemic tissue [2]. Paradoxically, while coronary reperfusion improves the prognosis of acute myocardial infarction, it also leads to myocardial reperfusion injury by extending myocardial damage within the ischemic period [3]. Studies in animal models of acute myocardial infarction show that reperfusion injury accounts for up to 50% of the final size of a myocardial infarct [4]. Therefore, intervention to alleviate reperfusion injury at the time of coronary recanalization has been considered to be the promising strategy to further decrease infarct size and improve the prognosis after myocardial infarction.

The accelerated generation of reactive oxygen species (ROS) by reperfusion of the ischemic myocardium is a potential mediator of reperfusion injury [5–7]. Many attempts have been made to inhibit ROS production to limit the extent of reperfusion injury. However, the administration of ROS scavengers at the time of reperfusion has produced conflicting results [8,9]. That can be partially explained by the dual role of ROS in ischemia-reperfused hearts. The majority of detrimental effects associated with lethal reperfusion injury are attributed to hydroxy radical ($^{\cdot}OH$), the most highly reactive oxygen species. By comparison, superoxide anion radical ($O_2^{\cdot-}$) and hydrogen peroxide (H_2O_2) have less oxidative energy and, paradoxically, are implicated as crucial signaling components in the establishment of favorable tolerance to oxidative stress upon ischemia–reperfusion [10,11]. Consequently, the inhibition of both pathways can be deleterious.

Recently, Ohsawa et al. demonstrated that molecular hydrogen (H_2) is a novel anti-oxidant with certain unique properties. (1) H_2 is permeable to cell membranes and can target organelles,

* Corresponding author. Address: Department of Regenerative Medicine and Advanced Cardiac Therapeutics, Keio University School of Medicine, 35 Shinanomachi Shinjuku-ku, Tokyo 160-8582, Japan. Fax: +81 3 5363 3875.
E-mail address: msano@sc.itc.keio.ac.jp (M. Sano).

0006-291X/$ - see front matter © 2008 Elsevier Inc. All rights reserved.
doi:10.1016/j.bbrc.2008.05.165

including mitochondria and nuclei; (2) H_2 specifically quenches exclusively detrimental ROS, such as $^{\cdot}OH$ and peroxynitrite ($ONOO^-$), while maintaining the metabolic oxidation–reduction reaction and other less potent ROS, such as $O_2^{\cdot-}$, H_2O_2, and nitric oxide ($NO^{\cdot}$); (3) inhalation of H_2 gas limits the infarct volume of brain and liver if given at the appropriate time during reperfusion [12,13]. However, clinical application of reperfusion therapy for these organs is limited. When translated into the clinical practice, H_2 gas inhalation therapy must be most frequently applied in the treatment of patients with acute myocardial infarction, since angioplastic recanalization of occluded infarct-related coronary artery is routinely performed.

The aim of this study was to investigate whether inhalation of H_2 gas exerts cardioprotective effects during myocardial ischemia–reperfusion. We showed the inhaled H_2 gas is rapidly transported and can reach even 'at risk' ischemic myocardium before coronary blood flow of the occluded infarct-related artery is reestablished. Inhalation of H_2 gas during ischemia and reperfusion significantly reduces infarct size without altering hemodynamic parameters, thereby preventing deleterious left ventricular (LV) remodeling.

Materials and methods

Animals. All experimental procedures and protocols were approved by the Animal Care and Use Committees of the Keio University and conformed to the NIH Guide for the Care and Use of Laboratory Animals. Eight-week-old male Wistar rats were artificially ventilated under anesthesia with ketamine (60 mg/kg) and xylazine (15 mg/kg) given intraperitoneally. Temperature was maintained at 37.5 ± 0.5 °C using a thermostatically controlled heating blanket connected to a thermometer probe placed in the rectum. H_2 gas was administered through a ventilator and the flow volume was controlled by a gas flowmeter TF-1 (YUTAKA Engineering Corporation, Tokyo, Japan). The concentration of H_2 in the gas mixture was determined using the Breath Gas Analyzer Model TGA-2000 (TERAMECS, Kyoto, Japan). Saturation of arterial oxygen level (SaO_2) was monitored by Clip sensor (PDR-43C) connected to Stand Alone Pulseoxymeter (CANL425SV). A Millar transducer catheter (SPR-320) was placed in the LV cavity via the left internal artery to monitor LV pressure using Polygraph system (NIHON KODEN; PEG-1000).

Myocardial ischemia–reperfusion model. Regional myocardial ischemia was induced by transient occlusion of the left anterior descending coronary artery. After 30 min of ischemia, we removed the tube for myocardial reperfusion and closed the thorax with the suture intact. The suture around the coronary artery was retied 24 h after reperfusion and 2% Evans blue dye was injected into the LV cavity to retrospectively delineate the area at risk of myocardial infarction. The heart was removed, washed in phosphate buffered saline, and then sliced into sequential 1 mm thick sections. We stained the sections with 2,3,5-triphenyltetrazolium chloride (TTC) (3%) then measured the infarct (white), non-infarct (red), non-ischemic, (blue), and at risk areas (AAR) (white and red).

Echocardiography. Rats were anesthetized by inhalation with 1.5% isoflurane. Animals were anchored to a positionable platform in a supine position. Short axis echocardiography was accomplished with a Vevo 660 system (VisualSonics) with the use of a 600 series real-time microvisualization scanhead probe.

Measurement of H_2 gas concentration. H_2 gas concentration was measured in tissues using a needle-type H_2 sensor (Unisense). The electrode current was measured with a picoammeter (Keithley) attached to a strip chart. The negative current obtained from the H_2 sensor was converted to regional H_2 concentration using a calibration curve generated from known levels of H_2 saturated saline.

Langendorff-perfusion of the heart. Hearts were excised quickly from heparinized Wistar male rats (350 g) and perfused with modified Krebs–Henseleit buffer (118 mmol/l NaCl, 25 mmol/l $NaHCO_3$, 4.7 mmol/l KCl, 1.2 mmol/l $MgSO_4$, 1.2 mmol/l KH_2PO_4, 1.75 mmol/l $CaCl_2$, 0.5 mmol/l EDTA, 11 mmol/l glucose, and 5 mmol/l pyruvate) equilibrated with a gas mixture comprised of 95% O_2/5% CO_2 at 37 °C. Coronary perfusion pressure was maintained at 70 mmHg. A plastic catheter with a latex balloon was inserted into the LV. Before the induction of anoxia, hearts were paced at 5 Hz, and the LV end-diastolic pressure was adjusted to 10 mmHg by filling the balloon with water. Pacing was turned off during anoxia and turn on 10, 20, 30, or 40 min after reoxygenation to measure the recovery of LV function. Indices of LV function [LV systolic pressure, LVSP; LV diastolic pressure, LVDP; LV developed pressure (LVDP = LVSP − LVDP); and LV peak positive and negative dP/dt] were recorded as described previously [14–17].

Immunohistochemical procedures. Sample fixation, embedding, sectioning, and blocking were performed as described previously [18]. Briefly, hearts were perfused from the apex with PBS, perfusion-fixed with 4% paraformaldehyde/PBS, dissected, subsequently cryoprotected in sucrose solutions at 4 °C, embedded in OCT compound (Miles Scientific, Naperville, IL), and quickly frozen in liquid nitrogen. The fixed hearts were sectioned (8 μm) using a CM3050S cryostat (Leica, Nussloch, Germany). For immunostaining, sections were blocked in 5% BSA for 30 min at room temperature and stained with anti-8OH-dG (MOG-020P; Japan Institute for the Control of Aging; 1:800) antibodies overnight at 4 °C. Secondary antibodies conjugated Alexa Fluor 546 (Molecular Probes, Eugene, OR, USA; 1:200) were applied for 1 h at 4 °C. Nuclei were stained with TO-PRO-3 (Molecular Probes) in a mounting medium. Slides were observed under Fluorescence Microscope (LYMPUS BX-60). The 8-OHdG positive area as percentage of total left ventricles at serial short axis sections was measured by planimetry using Image/J software from the National Institutes of Health (Bethesda, MD, USA).

Statistical analyses. Values are presented as means ± SEM. Statistical significance was evaluated using the unpaired Student's *t*-tests for comparisons between two mean values. Multiple comparisons between more than three groups were performed using ANOVA. A value of $P < 0.05$ was considered statistically significant.

Results

H_2 gas improves the recovery of left ventricular function during reoxygenation after anoxia in isolated perfused hearts

We first studied the effect of H_2 gas on the functional recovery after anoxia-reoxygenation in Langendorff-perfused rat hearts. Hearts were subjected to 40 min of anoxic perfusion with buffer equilibrated with either 100% N_2 (Control group) or 100% H_2 (H_2 group) followed by 40 min of aerobic reperfusion with buffer equilibrated with 95% O_2 and 5% CO_2 (Fig. 1A). H_2 gas significantly improved the recovery of LV developed pressure (LVDP), positive dP/dt, and negative dP/dt 40 min after reoxygenation ($n = 10$, $^*P < 0.05$, compared to control group, Fig. 1B).

Inhalation of H_2 gas immediately increases the intramyocardial H_2 gas concentration

Before we determined whether inhalation of hydrogen (H_2) gas confers cardioprotection against ischemia–reperfusion injury, the regional delivery of inhaled H_2 gas was investigated by monitoring the time-course of changes in H_2 levels using a needle-shaped

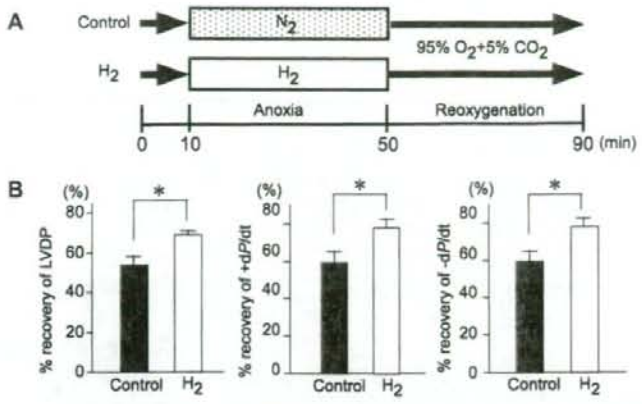

Fig. 1. H_2 gas improves the recovery of left ventricular function during reoxygenation after anoxia in isolated perfused hearts. (A) Experimental protocol of aoxia-reoxygenation. Isolated perfused rat hearts were subjected to 40 min of anoxia with buffer equilibrated with either 100% N_2 (control group) or 100% H_2 (H_2 group) followed by 40 min of aerobic reperfusion. (B) Comparison of percentage recovery of LVDP and peak positive and negative d*P*/d*t* 40 min after reoxygenation between control group and H_2 inhalation group ($n = 10$, $^*P < 0.05$, compared to control group).

hydrogen sensor electrode inserted directly into the tissues. When 2% H_2 gas was inhaled, the arterial H_2 levels started to increase 2 min after inhalation of H_2 gas and reached a maximum level after 5 min [1.82 ± 0.02% ($n = 5$)]. The incremental rate of H_2 saturation for the non-ischemic myocardium was similar to that observed in arterial blood with attaining a maximum of 1.73 ± 0.02% ($n = 5$) (Fig. 2A). By contrast, the rate of increase in the H_2 saturation was slower in the center of the thigh muscle with attaining a maximum level of 0.50 ± 0.03% ($n = 5$) after 30 min (Fig. 2B and Supplementary Fig.).

Of note, H_2 gas levels were increased even in the ischemic myocardium (Fig. 2C). Although the incremental rate of H_2 saturation was slower in the ischemic myocardium than in the non-ischemic myocardium, the peak level of H_2 in the ischemic myocardium was reached at approximately two thirds of the value observed in the non-ischemic myocardium (Fig. 2D). After restoration of coronary artery blood flow, the level of H_2 in the ischemic myocardium immediately increased to the level observed in the non-ischemic myocardium.

Inhalation of H_2 gas protects the heart from ischemia–reperfusion injury

To investigate whether inhalation of H_2 gas protects the heart from ischemia–reperfusion injury, rats were subjected to coronary artery occlusion for 30 min followed by reperfusion for 24 h. H_2 gas was administered at the onset of ischemia and continued for 60 min after reperfusion. H_2 gas has no adverse effect on heart rate and arterial oxygenation (Fig. 3A). There was no significant difference in the temporal profile of LV end-systolic

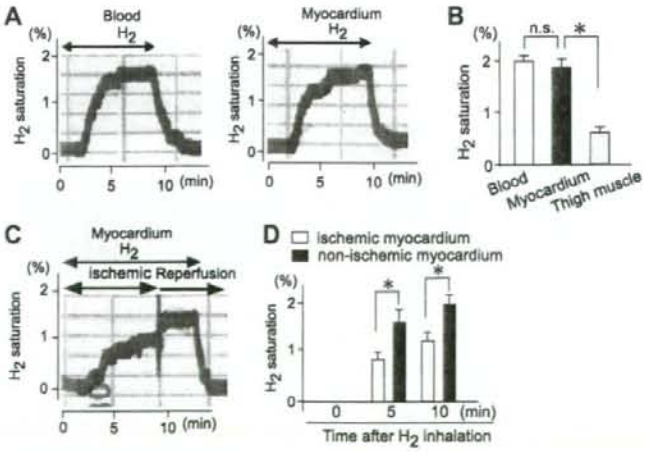

Fig. 2. Inhalation of H_2 gas increases the intramyocardial H_2 gas concentration. H_2 gas at 2% was administered by respiration to intubated rats receiving mechanical ventilation and the concentration of H_2 in tissue was recorded continuously. (A) A needle-type H_2 sensor was inserted in LV cavity (arterial blood) and non-ischemic LV myocardium. (B) Comparison of peak H_2 gas levels between arterial blood, non-ischemic LV myocardium, and thigh muscle ($n = 5$, $^*P < 0.05$, compared to the level of arterial blood). (C) The changes in the concentration of H_2 in 'at risk' area for infarction during ischemia and reperfusion. (D) Comparison of change in the H_2 concentration between non-ischemic and ischemic myocardium after H_2 inhalation ($n = 5$, $^*P < 0.05$, compared to the level of non-ischemic myocardium).

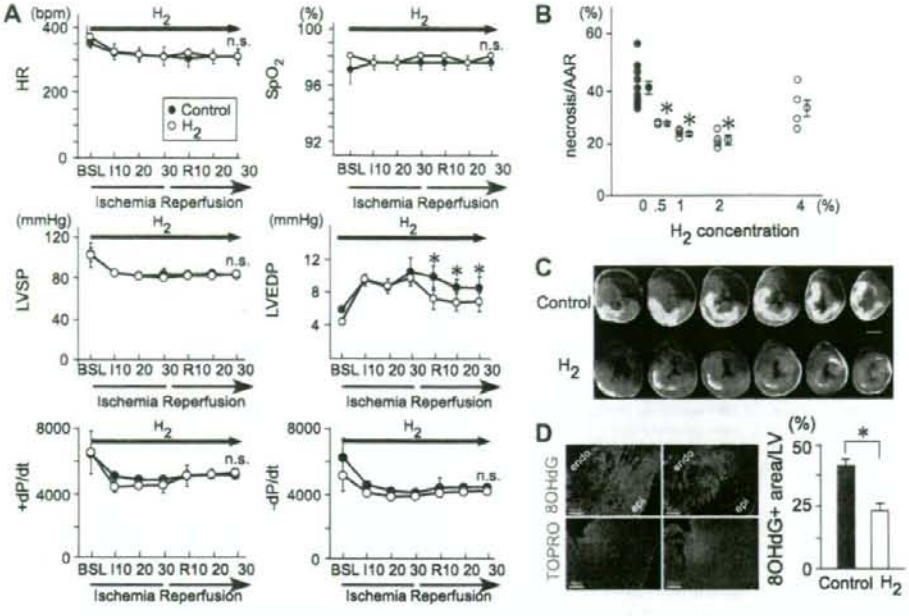

Fig. 3. Inhalation of H_2 reduces infarct size induced by ischemia–reperfusion injury. (A) Changes in heat rate (HR), oxygen saturation by pulse oximetry (SpO_2), and LV systolic pressure (LVSP), LV diastolic pressure (LVEDP) and LV peak positive and negative dP/dt were monitored during ischemia–reperfusion injury ($n = 5$ in each group). (B) H_2-dependent decrease in infarct size is expressed as the ratio of total infarct area/AAR ($^*P < 0.05$, compared to control group). (C) Representative photographs of serial heart sections obtained from rats subjected to myocardial ischemia–reperfusion injury in the presence or absence of H_2 inhalation. Bar = 2 mm. (D) Immunohistochemical staining with antibodies against 8-OHdG was performed 24 h after ischemia–reperfusion injury. Quantification of 8-OHdG immunoreactive area was expressed as percentage of total LV area at serial short axis sections ($n = 5$, $^*P < 0.05$, H_2 inhalation group compared to control group). endo, endocardium; epi, epicardium.

pressure, LV peak positive and negative LV dP/dt, between the control group and the 2% H_2 gas inhalation group. Notably, LV-end-diastolic pressure after reperfusion was significantly lower in H_2 gas inhalation group compared to control group ($n = 5$, $^*P < 0.05$).

In the absence of H_2 gas inhalation, infarct size following ischemia–reperfusion was 41.6 ± 2.5% of the area at risk ($n = 9$). By comparison, inhalation of 0.5–2% H_2 gas significantly reduced infarct size, with 2% H_2 gas providing the most prominent effects (21.2 ± 1.6% of area at risk, $n = 4$, Fig. 3B and C). There was no significant difference in area at risk/LV among control group and H_2 gas inhalation groups (data not shown). Consistent with those observations, the quantitative determination of 8-hydroxydeoxyguanosine (8-OHdG) immunoreactive area, a biomarker of oxidative stress, revealed that the level of oxidative injury elicited in the 'at risk' area was significantly smaller in the group receiving 2% H_2 gas inhalation than that of control group ($n = 5$, $^*P < 0.05$, Fig. 3D).

Inhalation of H_2 gas reduces LV remodeling after ischemia–reperfusion injury

To determine the impact of H_2 inhalation at the time of ischemia–reperfusion on pathological LV remodeling, LV morphology and function were monitored by echocardiography 30 days after myocardial ischemia–reperfusion injury. Control rats showed maladaptive pathological remodeling after myocardial infarction, including dilatation of LV cavity, reduced LV systolic function. Notably, inhalation of H_2 gas during myocardial ischemia–reperfusion reduced pathological remodeling after myocardial infarction (Fig. 4).

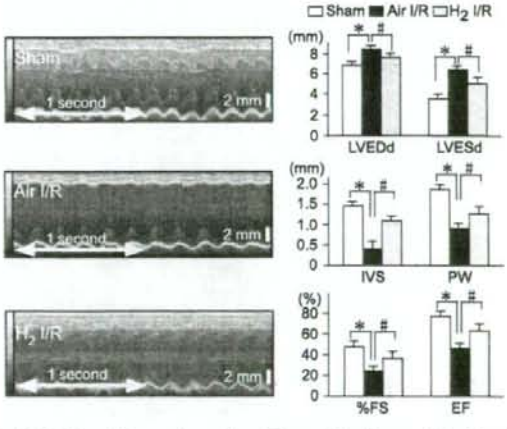

Fig. 4. Inhalation of H_2 gas reduces adverse LV remodeling. Representative M-mode echocardiographic images of sham-operated (sham), ischemia–reperfusion with air inhalation (Air_I/R), and ischemia–reperfusion with H_2 inhalation (H_2_I/R). Measurement of M-mode echocardiographic images in each group. LVEDd, LV endodiastolic diameter (μm); LVESd, LV endosystolic diameter (μm); IVC, intraventricular septum diameter (μm); PW, posterior wall thickness (μm); FS, fractional shortening (%); EF, ejection fraction (%) ($n = 5$, $^*P < 0.05$, compared to sham-operated group; $^\#P < 0.05$, compared to Air_I/R group).

Discussion

This is the first study to demonstrate that inhalation of H_2 gas, at an incombustible level, limit the extent of myocardial infarction

resulting from myocardial ischemia–reperfusion injury, and thereby preserve LV function *in vivo*. The cardioprotective effect of H_2 gas was also confirmed *ex vivo* Langendorff-perfused hearts subjected to anoxia-reoxygenation injury. The anti-oxidant properties of H_2 were confirmed by the demonstration that (1) H_2 improves the recovery of LV function during reoxygenation after anoxia, one of the oxidative stress model, in isolated perfused hearts; (2) inhalation of H_2 gas ameliorates the level of 8-OHdG immunoreactivity in the 'at risk' area for infarction. The anti-oxidant action of molecular H_2 may be explained, at least partially, by direct ROS scavenging effect. However, it remains unclear if the anti-oxidant action of H_2 is also ascribed to the activation of the reperfusion injury salvage kinase pathways or a direct effect on mitochondrial energetics.

Gas inhalation as disease therapy has received recent interest. There are three endogenous gas signaling molecules, known as gasotransmitters, include nitric oxide (NO), carbon monoxide (CO), and hydrogen sulfate (H_2S). The increased production of these gases under stress conditions may reflect the active involvement of these gases in the protective response. In pre-clinical experimental models of disease, including ischemia–reperfusion injury, the inhalation of exogenous CO or H_2S has produced a favorable outcome for most vital organs [19–22]. However, the inherent toxicity of these gases must be investigated for gas inhalation to be considered an effective therapeutic strategy. It is unknown if the therapeutically effective threshold for CO or H_2S can be attained locally in target organs without delivering a potentially toxic level of the gasses via the lungs.

H_2 is not produced endogenously in mammalian cells since the hydrogenase activity responsible for the formation of H_2 gas has not been identified [23]. The spontaneous production of H_2 gas in the human body occurs via fermentation of undigested carbohydrates by resident enterobacterial flora. H_2 is transferred to the portal circulation and excreted through the breath in significant amounts. We demonstrated that inhaled H_2 at therapeutic dose has no adverse effects on the saturation level of arterial oxygen (SpO_2) or hemodynamic parameters, including heart rate and LV pressure. H_2 dissolved in the blood is distributed to tissues proportional to regional blood flow, and is rapidly eliminated by the lungs. Accordingly, the H_2 gas clearance method was employed to measure local blood flow in various tissues [24]. Since the heart is one of the most highly perfused tissues, the intramyocardial H_2 concentration increases immediately following inhalation of H_2, and attaining to almost compatible levels of that observed in arterial blood within 10 min. Of note, the regional H_2 concentration in the ischemic myocardium reaches at two thirds of the value observed in the non-ischemic myocardium. This may occur through gaseous diffusion from the blood in the ventricular cavity and/or adjacent non-ischemic myocardium. These findings indicate that administration of H_2 gas by inhalation, in patients with totally coronary artery occlusion, can efficiently increase the regional concentration of H_2 in the 'at risk' area for myocardial infarction before reestablishing coronary blood flow within the occluded infarct-related artery.

We demonstrated that inhalation of H_2 gas is promising strategies to alleviate ischemia–reperfusion injury at the time of recanalization of coronary artery. When translated into the clinical practice, inhalation of H_2 gas must be most frequently applied in the treatment of patients with acute myocardial infarction in conjunction with routinely performed PCI procedures. Further understanding of the mechanisms underlying the signaling pathways involved in H_2-mediated anti-oxidant activity, and the capacity of H_2 to influence cellular metabolism, is required to fully exploit inhalation of H_2 gas as a therapeutic strategy.

Acknowledgments

We thank M. Okada (NIHON KODEN), S. Kotouda (LMS laboratory and Medical Supplies), C. Ogawa, K. Nishimaki, M. Kamimura, M. Abe, Y. Miyake, H. Kawaguchi, H. Shiozawa, and M. Ono for their technical assistance. M. Sano is a core member of the Global Center-of-Excellence (GCOE) for Human Metabolomics Systems Biology from MEXT. This work was supported by a PRESTO (Metabolism and Cellular Function) grant from the Japanese Science and Technology Agency awarded to M. Sano.

Appendix A. Supplementary data

Supplementary data associated with this article can be found, in the online version, at doi:10.1016/j.bbrc.2008.05.165.

References

[1] A. Volpi, C. De Vita, M.G. Franzosi, E. Geraci, A.P. Maggioni, F. Mauri, E. Negri, E. Santoro, L. Tavazzi, G. Tognoni, Determinants of 6-month mortality in survivors of myocardial infarction after thrombolysis. Results of the GISSI-2 data base. The Ad hoc Working Group of the Gruppo Italiano per lo Studio della Sopravvivenza nell'Infarto Miocardico (GISSI)-2 Data Base, Circulation 88 (1993) 416–429.
[2] E.C. Keeley, J.A. Boura, C.L. Grines, Primary angioplasty versus intravenous thrombolytic therapy for acute myocardial infarction: a quantitative review of 23 randomised trials, Lancet 361 (2003) 13–20.
[3] E. Braunwald, R.A. Kloner, Myocardial reperfusion: a double-edged sword?, J Clin. Invest. 76 (1985) 1713–1719.
[4] D.M. Yellon, D.J. Hausenloy, Myocardial reperfusion injury, N. Engl. J. Med. 357 (2007) 1121–1135.
[5] J.L. Zweier, Measurement of superoxide-derived free radicals in the reperfused heart. Evidence for a free radical mechanism of reperfusion injury, J. Biol. Chem. 263 (1988) 1353–1357.
[6] R. Bolli, B.S. Patel, M.O. Jeroudi, E.K. Lai, P.B. McCay, Demonstration of free radical generation in "stunned" myocardium of intact dogs with the use of the spin trap alpha-phenyl *N*-*tert*-butyl nitrone, J. Clin. Invest. 82 (1988) 476–485.
[7] T. Vanden Hoek, L.B. Becker, Z.H. Shao, C.Q. Li, P.T. Schumacker, Preconditioning in cardiomyocytes protects by attenuating oxidant stress at reperfusion, Circ. Res. 86 (2000) 541–548.
[8] J.T. Flaherty, B. Pitt, J.W. Gruber, R.R. Heuser, D.A. Rothbaum, L.R. Burwell, B.S. George, D.J. Kereiakes, D. Deitchman, N. Gustafson, et al., Recombinant human superoxide dismutase (h-SOD) fails to improve recovery of ventricular function in patients undergoing coronary angioplasty for acute myocardial infarction, Circulation 89 (1994) 1982–1991.
[9] V.J. Richard, C.E. Murry, R.B. Jennings, K.A. Reimer, Therapy to reduce free radicals during early reperfusion does not limit the size of myocardial infarcts caused by 90 minutes of ischemia in dogs, Circulation 78 (1988) 473–480.
[10] C. Penna, R. Rastaldo, D. Mancardi, S. Raimondo, S. Cappello, D. Gattullo, G. Losano, P. Pagliaro, Post-conditioning induced cardioprotection requires signaling through a redox-sensitive mechanism, mitochondrial ATP-sensitive K^+ channel and protein kinase C activation, Basic Res. Cardiol. 101 (2006) 180–189.
[11] J.M. Downey, M.V. Cohen, A really radical observation—a comment on Penna et al., Basic Res. Cardiol. 101 (2006) 190–191.
[12] I. Ohsawa, M. Ishikawa, K. Takahashi, M. Watanabe, K. Nishimaki, K. Yamagata, K. Katsura, Y. Katayama, S. Asoh, S. Ohta, Hydrogen acts as a therapeutic antioxidant by selectively reducing cytotoxic oxygen radicals, Nat. Med. 13 (2007) 688–694.
[13] K. Fukuda, S. Asoh, M. Ishikawa, Y. Yamamoto, I. Ohsawa, S. Ohta, Inhalation of hydrogen gas suppresses hepatic injury caused by ischemia/reperfusion through reducing oxidative stress, Biochem. Biophys. Res. Commun. 361 (2007) 670–674.
[14] M. Tani, Y. Suganuma, H. Hasegawa, K. Shinmura, Y. Hayashi, X. Guo, Y. Nakamura, Changes in ischemic tolerance and effects of ischemic preconditioning in middle-aged rat hearts, Circulation 95 (1997) 2559–2566.
[15] K. Shinmura, K. Tamaki, R. Bolli, Short-term caloric restriction improves ischemic tolerance independent of opening of ATP-sensitive K^+ channels in both young and aged hearts, J. Mol. Cell. Cardiol. 39 (2005) 285–296.
[16] K. Shinmura, K. Tamaki, K. Saito, Y. Nakano, T. Tobe, R. Bolli, Cardioprotective effects of short-term caloric restriction are mediated by adiponectin via activation of AMP-activated protein kinase, Circulation 116 (2007) 2809–2817.
[17] J.P. Headrick, Aging impairs functional, metabolic and ionic recovery from ischemia–reperfusion and hypoxia–reoxygenation, J. Mol. Cell. Cardiol. 30 (1998) 1415–1430.
[18] J. Endo, M. Sano, J. Fujita, K. Hayashida, S. Yuasa, N. Aoyama, Y. Takehara, O. Kato, S. Makino, S. Ogawa, K. Fukuda, Bone marrow derived cells are involved in the pathogenesis of cardiac hypertrophy in response to pressure overload, Circulation 116 (2007) 1176–1184.

[19] C. Szabo, Hydrogen sulphide and its therapeutic potential, Nat. Rev. Drug Discov. 6 (2007) 917–935.
[20] J.W. Elrod, J.W. Calvert, J. Morrison, J.E. Doeller, D.W. Kraus, L. Tao, X. Jiao, R. Scalia, L. Kiss, C. Szabo, H. Kimura, C.W. Chow, D.J. Lefer, Hydrogen sulfide attenuates myocardial ischemia-reperfusion injury by preservation of mitochondrial function, Proc. Natl. Acad. Sci. USA 104 (2007) 15560–15565.
[21] R. Foresti, M.G. Bani-Hani, R. Motterlini, Use of carbon monoxide as a therapeutic agent: promises and challenges, Intensive Care Med. (2008).
[22] A. Kobayashi, K. Ishikawa, H. Matsumoto, S. Kimura, Y. Kamiyama, Y. Maruyama, Synergetic antioxidant and vasodilatory action of carbon monoxide in angiotensin II-induced cardiac hypertrophy, Hypertension 50 (2007) 1040–1048.
[23] M.W. Adams, L.E. Mortenson, J.S. Chen, Hydrogenase, Biochim. Biophys. Acta 594 (1980) 105–176.
[24] K. Aukland, B.F. Bower, R.W. Berliner, Measurement of local blood flow with hydrogen gas, Circ. Res. 14 (1964) 164–187.

Journal of Neurochemistry

JNC

JOURNAL OF NEUROCHEMISTRY | 2008 | 106 | 258–270 doi: 10.1111/j.1471-4159.2008.05360.x

Combination therapy with transductive anti-death FNK protein and FK506 ameliorates brain damage with focal transient ischemia in rat

Ken-ichiro Katsura,* Kumiko Takahashi,* Sadamitsu Asoh,† Megumi Watanabe,*,† Makoto Sakurazawa,* Ikuroh Ohsawa,† Takashi Mori,‡ Hironaka Igarashi,* Seiji Ohkubo,* Yasuo Katayama* and Shigeo Ohta†

*Department of Internal Medicine, Nippon Medical School, Tokyo, Japan

†Department of Biochemistry and Cell Biology, Institute of Development and Aging Sciences, Graduate School of Medicine, Nippon Medical School, Kawasaki, Japan

‡Saitama Medical Center/School, Kawagoe, Saitama, Japan

Abstract

Many practical therapies have been explored as clinical applications for ischemic cerebral infarction; however, most are still insufficient to treat acute stroke. We show here a potential combination therapy in a rat focal ischemic model to improve neurological symptoms as well as to reduce infarct volumes at the maximum level. We applied protein transduction technology using artificial anti-death Bcl-x_L derivative with three amino acid-substitutions (Y22F, Q26N and R165K) (FNK) protein fused with a protein-transduction-domain peptide (PTD-FNK). When PTD-FNK was administrated 1 h after initiating ischemia followed by the administration of an immunosuppressant FK506 with a 30-min time lag, infarct volumes of the total brain and cortex were markedly reduced to 27% and 14%, respectively. This procedure not only reduced the infarct volume and edema, but also markedly improved neurological symptoms. The therapeutic effect continued for at least 1 week after ischemia. FK506 inhibited the transduction of PTD-FNK *in vitro*, which explains the requirement of a time lag for the administration of FK506. An additional *in vitro* experiment showed that PTD-FNK, when administered 30 min before FK506, gave the maximal protective effect by reducing the intracellular calcium concentration. We propose that this combination therapy would provide a synergistic protective effect by both drugs, reducing adverse the effects of FK506.

Keywords: Bcl-2 family, calcium movement, FK506, protein transduction, stroke.

J. Neurochem. (2008) **106**, 258–270.

The delivery of therapeutic materials into the brain is severely limited by the blood–brain barrier. Gene therapy may be a potential technology to overcome this problem; however, it takes considerable time to deliver a gene of interest into the brain and to express a sufficient amount of therapeutic protein, suggesting that this technology may not be suitable for emergent treatments. As an alternative approach, delivering therapeutic proteins directly to ischemic brain tissue through a protein transduction domain (PTD) has been proposed (Schwarze *et al.* 1999; Wadia and Dowdy 2002). PTD has made it possible to design strategies for delivering pharmacologically potent macromolecules and even active enzymes to brain tissue by crossing the blood–brain barrier and cell membranes (Denicourt and Dowdy 2003).

Anti-apoptotic members of the Bcl-2 family, Bcl-2 and Bcl-x_L, would be appropriate candidates for protein therapeutics (Reed 1997; vander Heiden and Thompson

Received September 5, 2007; revised manuscript received March 2, 2008; accepted March 13, 2008.

Address correspondence and reprint requests to Shigeo Ohta, Department of Biochemistry and Cell Biology, Institute of Development and Aging Sciences, Graduate School of Medicine, Nippon Medical School, 1-396 Kosugi-cho, Nakahara-ku, Kawasaki-city, Kanagawa 211-8533, Japan. E-mail: ohta@nms.ac.jp

Abbreviations used: ADC, apparent diffusion coefficient; CBF, cerebral blood flow; ER, endoplasmic reticulum; FNK, Bcl-x_L derivative with three amino acid-substitutions (Y22F, Q26N and R165K); MCA, middle cerebral artery; PTD, protein transduction domain; rCBF, Regional CBF; TG, thapsigargin.

1999). To enhance their cytoprotective activity, we constructed a powerful artificial cytoprotective protein, FNK (originally referred as Bcl-xFNK in Asoh et al. 2000), from Bcl-x_L by site-directed mutagenesis of three amino acid residues (Y22F/ Q26N/ R165K) (Asoh et al. 2000, 2002). FNK is the first mutant with a gain-of-function phenotype among the mammalian anti-apoptotic factors and showed anti-necrotic as well as anti-apoptotic activity (Asoh *et al.* 2000, 2005). In fact, pre-treatment with PTD-FNK, administered intraperitoneally in gerbils, prevented delayed neuronal death in the hippocampus caused by transient global ischemia (Asoh *et al.* 2002), suggesting that PTD-FNK has potential as a therapeutic agent against ischemic stroke. PTD-FNK may have potential for various medical applications: it protected various cells from cell death induced by Fas antibody and nitrogen oxide (Ozaki *et al.* 2004), by carbon tetrachloride (Asoh *et al.* 2005), by freezing and thawing (Sudo *et al.* 2005), by aminoglycoside toxicity (Kashio *et al.* 2007), and by lipopolysaccharide (Chen *et al.* 2007). Moreover, PTD-FNK improved the efficacy of bone marrow mononuclear cell transplantation (Tara *et al.* 2007), protected rat hearts from myocardial infarction (Arakawa *et al.* 2007), and prevented chemotherapy-induced alopecia (Nakashima-Kamimura *et al.* 2008). It is expected that PTD-FNK would be useful as actual therapy for cerebral ischemic disease; however, the effect of PTD-FNK on focal ischemia has not yet been investigated. We proceeded with experiments using a focal ischemic model in rats to prevent brain injury after transient focal ischemia by the post-administration of PTD-FNK.

FK506 (Tacrolimus) is an immunosuppressant to prevent allograft rejection after organ transplantation. In addition, FK506 has a protective effect against ischemia-reperfusion injury in organs, including the heart (Nishinaka *et al.* 1993), liver (Garcia-Criado *et al.* 1997; Matsuda *et al.* 1998), and kidney (Sakr *et al.* 1992). After Sharkey and Butcher (1994) first showed that post ischemic administration of FK506 mitigates brain injury following permanent ligation of the rat middle cerebral artery (MCA), many studies have confirmed the neuroprotective effect of FK506 in various experimental models, including a focal ischemia model using a filament (Kuroda and Siesjö 1996; Arii *et al.* 2001) and a transient global ischemia model (Drake *et al.* 1996; Ide *et al.* 1996; Yagita *et al.* 1996; Katsura *et al.* 2003). In addition, FK506 is shown to display a neurotrophic effect (Gold *et al.* 1994; Lyons *et al.* 1994).

It is estimated that there are 730 000 and 1 500 000 initial strokes each year in the United States and Japan, respectively, and that stroke is the third leading cause of death in many countries (Warlow 1998). Moreover, about 40% of bedridden aged people who are hospitalized in Japan are bedridden because of stroke (Ministry of Health, Labour and Welfare, Japan 2002), which makes stroke the leading cause of increasing medical expenses.

Recently, with progress in new therapeutic approaches, a worldwide campaign was initiated to enlighten patients in the very early stages of stroke (the 'Brain Attack' campaign), and numerous new drugs have been put through clinical trials, despite little success; however, there have been few trials of combination therapies with two or more effective drugs. An exploration of treatment methods using a combination of several carefully selected neuroprotective drugs with different time courses is greatly anticipated (de Keyser *et al.* 1999).

We explored the potential of a therapy combining PTD-FNK and FK506, and obtained striking protective effects with time-lag combination therapy. These pre-clinical observations may provide a foundation for future clinical trials.

Materials and methods

Animal model

Male Sprague-Dawley rats (250–300 g) were anesthetized with halothane (4% for induction, 1% for maintenance) in nitrous oxide/oxygen (70%/30%, v/v). Temperature (37.5 ± 0.5°C) was maintained using a thermostatically controlled heating blanket connected to a thermometer probe in the rectum. The tail artery and vein were cannulated for monitoring physiological parameters and for drug infusion, respectively. Focal ischemia was produced by intraluminal occlusion of the left MCA with a nylon monofilament with a rounded tip and a distal silicon rubber cylinder (Arii *et al.* 2001; Ohsawa *et al.* 2007). The animals underwent MCA occlusion for 90 min and then reperfusion. After recovering from anesthesia, the animals were maintained in an air-conditioned room at 20°C. Animal protocols were approved by the Animal Care and Use Committee of Nippon Medical School. Experiments were performed in a blinded fashion by an examiner.

Determination of infarct and edema volume

At 24 h after MCA occlusion, the brain was removed and sliced into six coronal sections (2 mm thick). All six sections were stained with 3% of 2,3,5-triphenyltetrazolium chloride, which is reduced to an insoluble crimson-colored formazan by mitochondrial dehydrogenases. After taking digital images of all sections to evaluate infarct volume, they were analyzed with NIH IMAGE software. The border between infarct and non-infarct tissues in each section was outlined using an image analysis system, and the area of infarction was estimated by subtracting the non-lesioned area of the ipsilateral hemisphere from that of the contralateral side (Swanson *et al.* 1990) in a blinded fashion. The volume of infarction was calculated by integration of the lesioned areas. The increase in brain volume caused by edema was measured by subtracting the area of the non-lesioned contralateral hemisphere from that of the ipsilateral lesioned hemisphere. Edema volume was also calculated by integration.

Evaluation of infarct volume at 1 week after ischemia

One week after MCA occlusion, rats were anesthetized again and killed. Brains were quickly removed and frozen by immersion in chilled isopentane (−40°C). Frozen brains were sliced into 20-μm sections on a cryostat (Clinicut, Bright Instrument Company